

Bacterial filamentation: a bet for survival in stressful environments



Jesús Vélez Santiago
Center for Genomic Sciences
National Autonomous University of Mexico

A thesis submitted for the degree of

Bachelor of Science

Cuernavaca, Morelos, Mexico - 2021-08

For Yihui Xie

Acknowledgements

Lorem ipsum dolor sit amet, consectetur adipiscing elit. Integer tristique, sem egestas aliquam varius, arcu nisi ullamcorper lacus, quis convallis enim velit et arcu. Vestibulum lacus arcu, tempor non dapibus vitae, malesuada ut ipsum. Phasellus condimentum diam ex. Sed maximus a mauris vel aliquet.

Integer neque sapien, cursus eu viverra consequat, cursus congue dui. Maecenas est dui, rutrum vitae enim vel, varius scelerisque tortor. In vel dignissim orci. Integer varius neque mauris, mollis commodo libero fringilla sed. Nunc accumsan, libero id interdum dignissim, nulla nibh consectetur lorem, vel dignissim erat magna vitae ante. Aliquam at est lectus. Suspendisse nec sem euismod, condimentum neque sit amet, malesuada nibh. Aenean condimentum pharetra quam, id venenatis mauris tempor a.

Jesús Vélez Santiago
Center for Genomic Sciences
2021, 08

Abstract

Etiam venenatis purus eu felis viverra sodales. Sed et varius ex. Nullam sit amet aliquet purus. Fusce elementum vitae est eget vulputate. Aliquam erat volutpat. Donec ac suscipit leo, sed euismod nisi. Duis malesuada elementum pulvinar. Ut et vulputate augue. In dignissim ligula at nulla feugiat cursus. Suspendisse sed diam ut ligula sollicitudin pellentesque. Etiam ut gravida velit, vitae lobortis mi. Nam congue laoreet mauris sit amet iaculis.

Contents

List of Figures	vi
List of Tables	viii
List of Abbreviations	ix
Introduction	1
1 Experiment analysis	2
1.1 Introduction	2
1.2 Experiment design	2
1.3 Exploratory Data Analysis	2
1.4 Discussion	25
2 Models to the rescue; filamentation abstraction	26
2.1 Introduction	27
2.2 Filamentation model	28
2.3 Results	29
2.4 Discussion	35
3 Discussion	36
Appendices	
A The First Appendix	38
Works Cited	39

List of Figures

1.1	Cell classification and its distribution across experiments.	4
1.2	Cells life time classes distribution.	5
1.3	Cell's number of divisions.	6
1.4	Time elapsed since the last division at the beginning of the experiment.	7
1.5	Experiment initial values.	8
1.6	Experiment initial values differences.	9
1.7	Principal Component Analysis of chromosomal strain.	10
1.8	Variables contribution of Principal Component Analysis of chromosomal strain.	11
1.9	Principal Component Analysis of plasmid strain.	12
1.10	Variables contribution of Principal Component Analysis of plasmid strain.	13
1.11	UMAP coordinates of chromosome strain.	14
1.12	UMAP coordinates of plasmid strain.	15
1.13	DS-red temporal distribution.	16
1.14	GFP temporal distribution.	17
1.15	Length temporal distribution.	18
1.16	Time to filamentation without filters.	18
1.17	Time to filamentation filtered.	19
1.18	Experiment initial values differences with time.	19
1.19	Experiment initial values with time.	20
1.20	Population measurements over time.	21
1.21	Plasmid initial GFP survival probability.	22
1.22	Plasmid initial length survival probability.	22
1.23	Population status over time without dead.	23
1.24	Population status over time with dead.	23
1.25	Population survivals binned by initial GFP over time.	24
1.26	Normalized population survivals binned by initial GFP over time.	24

List of Figures

2.1	Cell dimensions relationship.	28
2.2	Effect of filamentation on intracellular toxin concentration.	30
2.3	Effect of filamentation on minimum inhibitory concentration (MIC).	32
2.4	Variability in the toxin-antitoxin system produces different proportions of cell states.	33
2.5	Effect of variability on the toxin-antitoxin system.	34

List of Tables

List of Abbreviations

- 1-D, 2-D** . . . One- or two-dimensional, referring **in this thesis** to spatial dimensions in an image.
- Otter** One of the finest of water mammals.
- Hedgehog** . . . Quite a nice prickly friend.

Introduction

1

Experiment analysis

Contents

1.1	Introduction	2
1.2	Experiment design	2
1.3	Exploratory Data Analysis	2
1.3.1	General preprocessing of data	2
1.3.2	Cells level	4
1.3.3	Tracks level	21
1.4	Discussion	25

1.1 Introduction

1.2 Experiment design

1.3 Exploratory Data Analysis

1.3.1 General preprocessing of data

The processing of the raw data consisted mainly of creating two levels of observation for the cells of both chromosomal strains and multicopy plasmids. The first level is at a cell granularity, that is, point properties. The second level consists of the cells over time, thus observing properties at the population level. We did this because it

1. Experiment analysis

would allow us to understand what factors are affecting filamentation and why.

We decided to normalize the fluorescence values of DS-Red and GFP for both

experiments based on the values observed before the start of the experiment. It

allowed us to have a basis to work with and compare the expressions between cells.

In the case of DS-Red, we also applied a logarithmic transformation to observe

subtle changes that would allow us to dig deeper.

Ultimately, we decided to classify cells into four fundamental groups based on

whether the cell was filamented and survived (see 1.1). We define a *filamented*

cell as a cell that is more than two standard deviations from the mean concerning

the lengths observed before antibiotic entry into the system []. On the other

hand, although there are multiple ways to define death in a cell context [], we

decided to consider a *cell dead or missing* when we stopped having information

about it, either because of its fluorescence levels or because it left the field of

experimental tracking. Therefore, a *surviving cell* is one that existed before and

after the exposure to the antibiotic.

1. Experiment analysis

1.3.2 Cells level

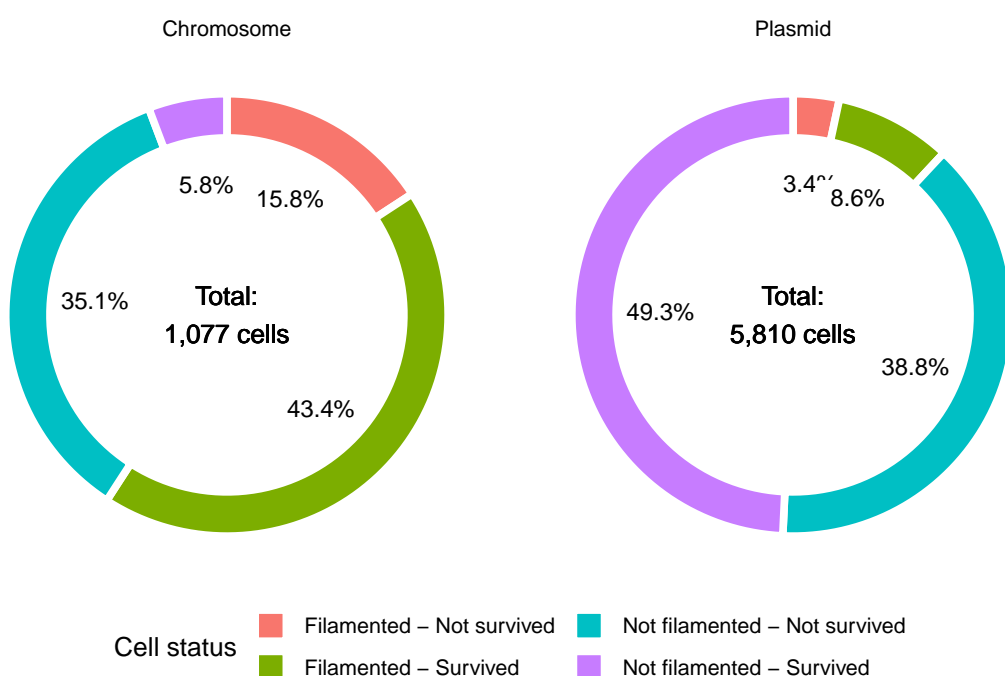


Figure 1.1: Cell classification and its distribution across experiments. We define a *filamented cell* as a cell whose length exceeded two standard deviations from the mean at any time during the experiment. A *surviving cell* is a cell that existed before and after exposure to the antibiotic. We removed from the analysis those cells that died before or were born after the exposure of the experiment. Therefore, we delimited the effect caused by the exposure to the antibiotic.

1. Experiment analysis

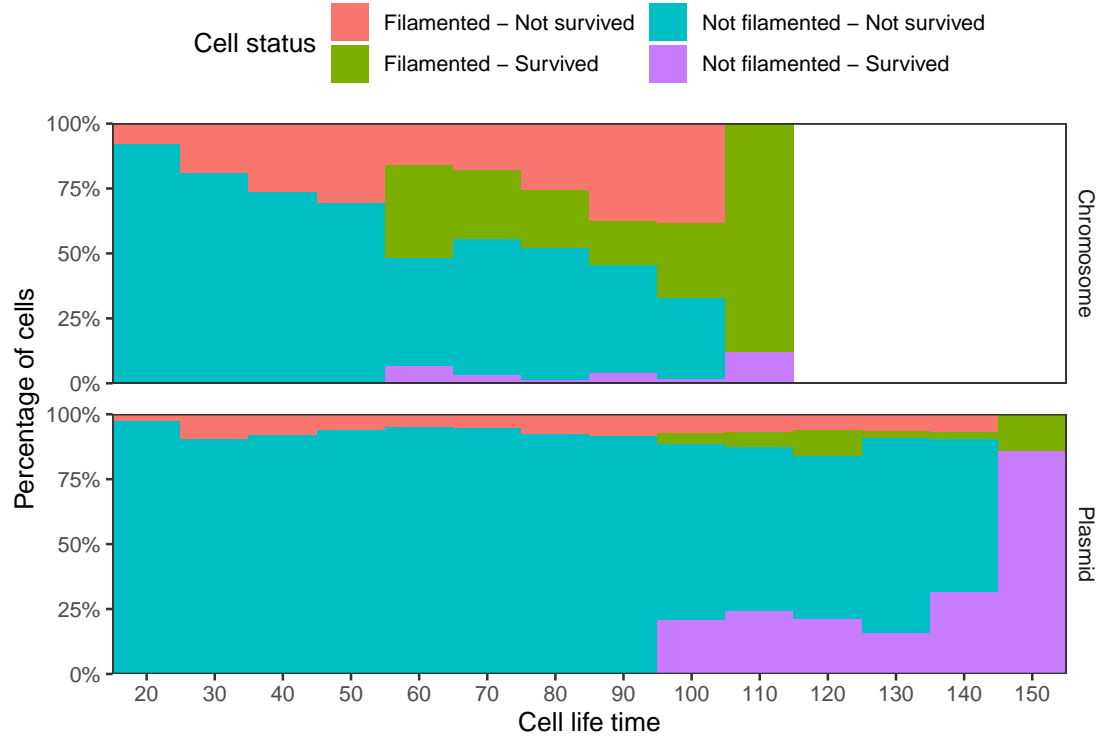


Figure 1.2: Cells life time classes distribution. Chromosomal cells appear to show more remarkable survival by the filamented class compared to non-filamented survivors. On the other hand, in cells with plasmids, the relationship seems to be the opposite. However, this may be due to several factors. For instance, the levels of antibiotic resistance inherent in a heterogeneous population is the most simple explanation. For each cell, we calculate its lifetime, that is, the last time we saw the cell minus the time we had our first observation of it. We truncated the time to one frame (*i.e.*, 10 minutes) after finishing the antibiotic exposure. From the first appearance of green or purple color (*i.e.*, surviving cells), higher lifetime values represent cells that existed long before the start of the experiment.

1. Experiment analysis

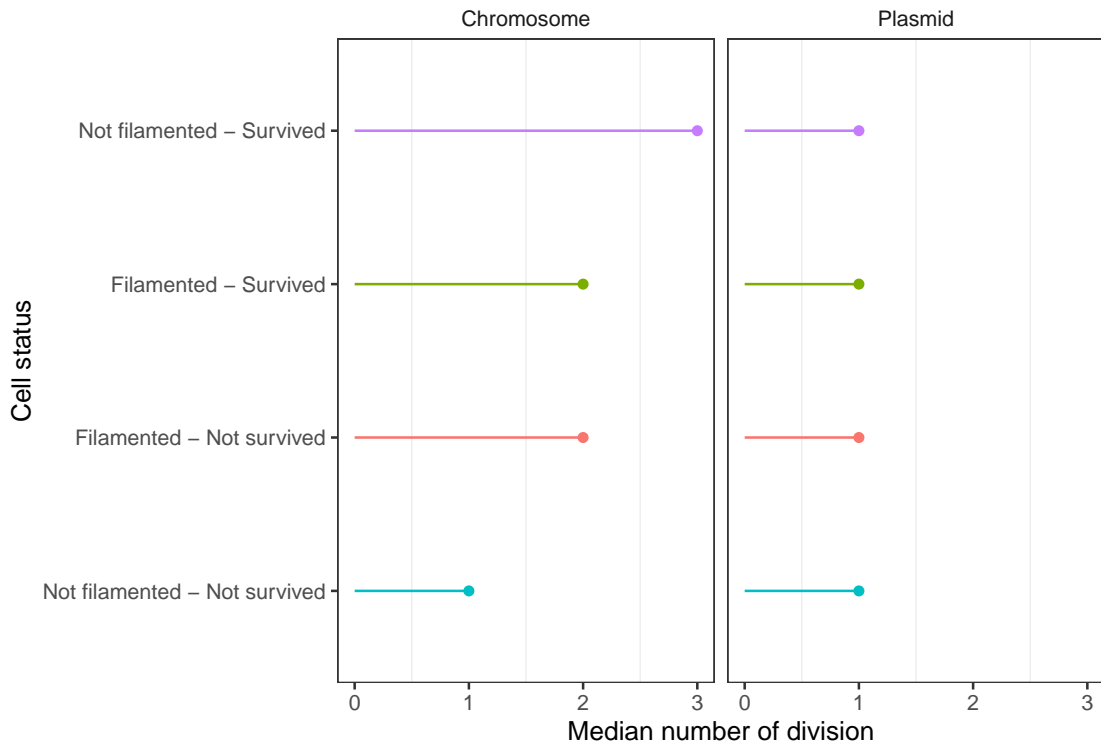


Figure 1.3: Cell's number of divisions. Chromosomal cells exhibited more divisions for surviving classes and non-surviving filamented cells (*i.e.*, purple, green, and red dots) relative to unchanged behavior in plasmid cells. Therefore, its contribution to filamentation remains uncertain.

1. Experiment analysis

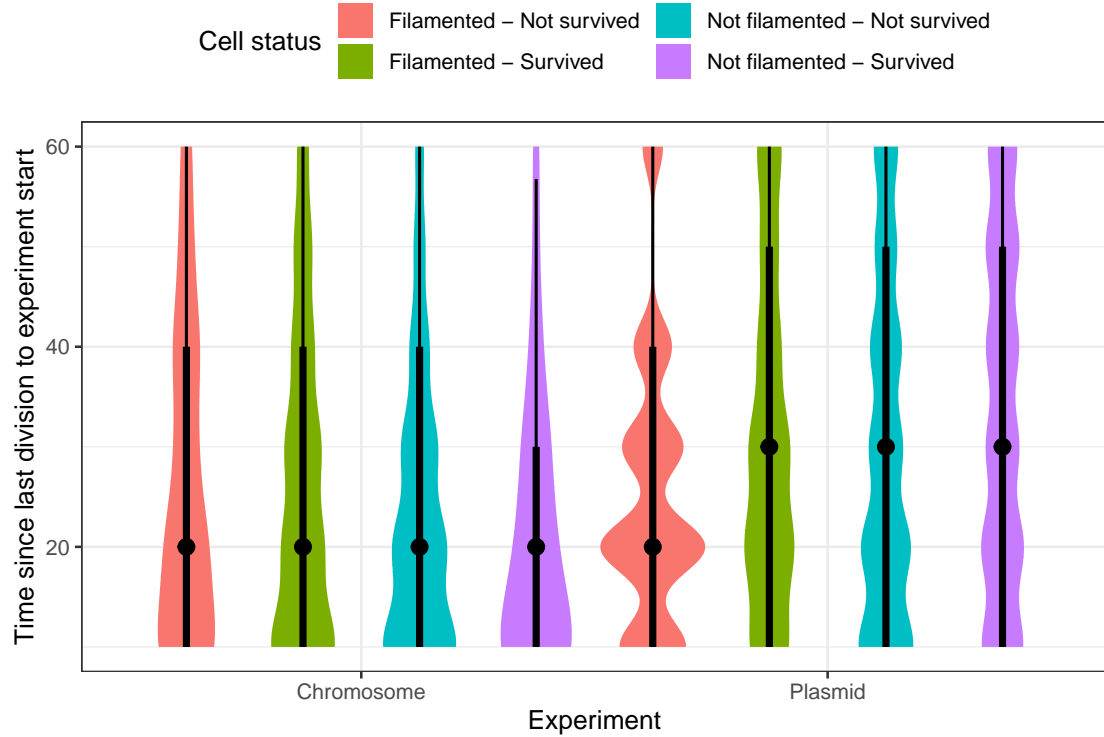


Figure 1.4: Time elapsed since the last division at the beginning of the experiment. The mean time of the last division before starting the experiment indicates that it did not influence the final result for chromosomal cells. There is a slight difference between the filamented-not survived cells and the rest of the classes for cells with plasmids. However, the signal does not appear to be strong on the survival role. Therefore, we conclude that we have no evidence to support that the time of the last division at the beginning of the experiment influences the final classification results.

1. Experiment analysis

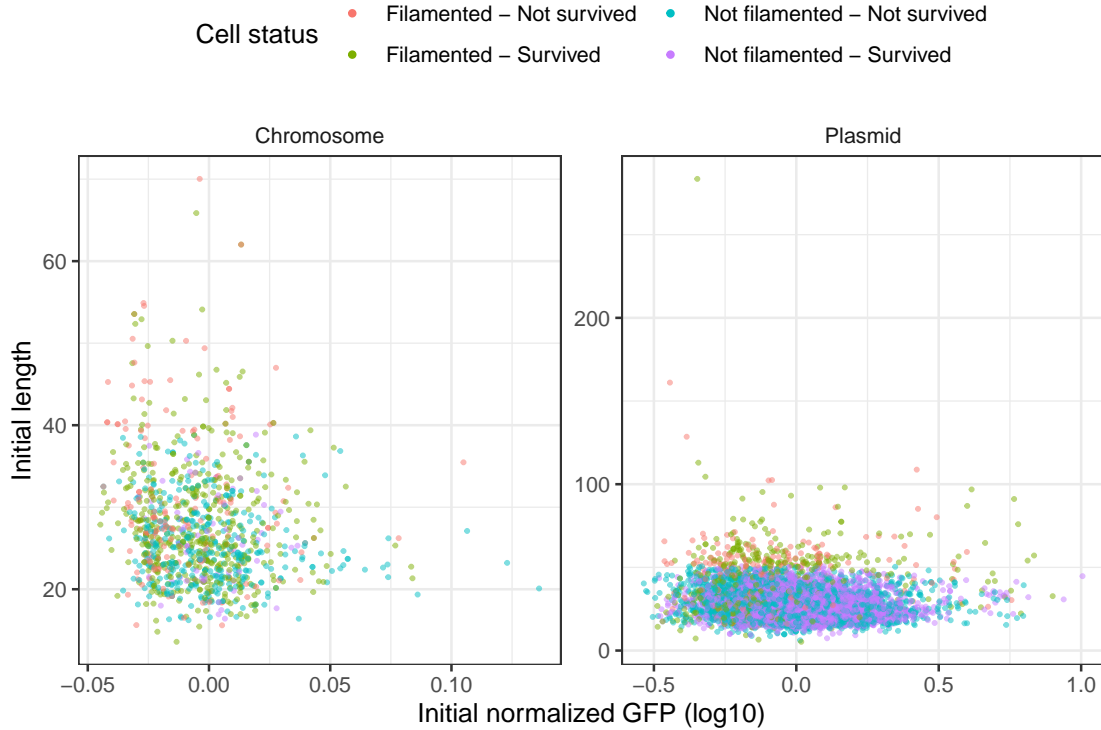


Figure 1.5: Experiment initial values. By positioning a cell in space based on its initial length and GFP values, we can see that class separation occurs, but not as a strong signal. Therefore, we concluded that although the initial state influences the result, this is not everything. For this, we have the example of the length changes throughout the experiment caused by filamentation. In this graph, the GFP scale is at log10 to help us observe those minor differences between the experiments.

1. Experiment analysis

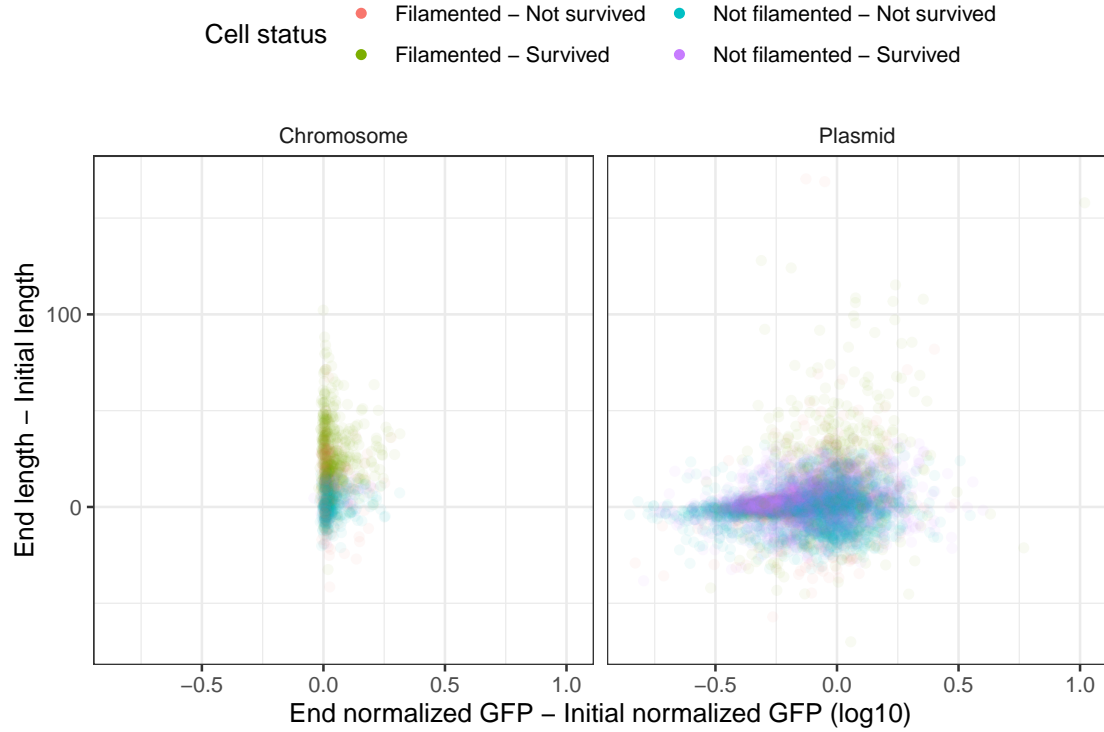


Figure 1.6: Experiment initial values differences. By comparing the metric differences of the last observation and the first observation of a cell, we can separate mainly the surviving filamented cells from those that did not do it in both experiments (green dots). Meanwhile, cells with plasmids form a small accumulation of surviving cells that did not produce filament (purple dots). However, this has made a breakthrough in understanding what is affecting cell survival. There are still variables that we can include to understand this phenomenon better.

1. Experiment analysis

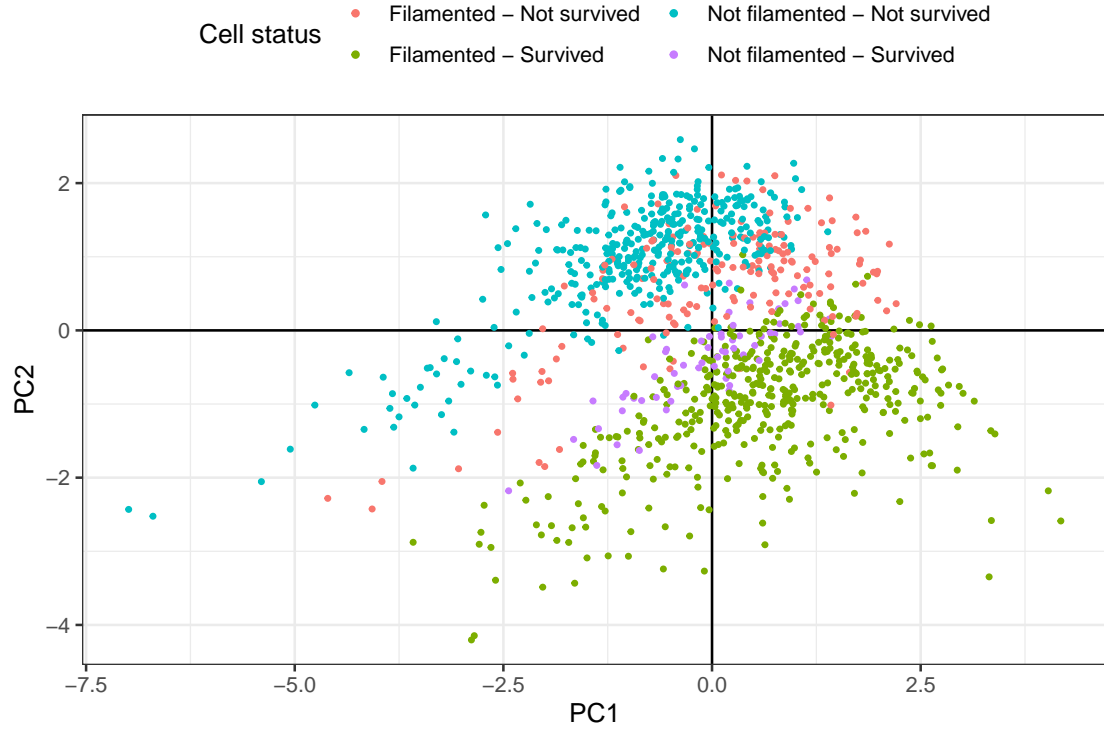


Figure 1.7: Principal Component Analysis of chromosomal strain. When integrating the information of different variables in a dimensionality reduction analysis, we observed a clear separation between the surviving cells and those that did not. The contributions that determined this phenomenon come mainly from the last amount of DS-red, GFP, and length of the cell (see Figure 1.8). Although it seems obvious, it effectively confirms that the temporal classification that we carry out makes sense. Thus, highlighting the importance of filamentation. Longer length represents a greater uptake of antibiotics but in a much larger volume, so the net effect is an internal reduction of antibiotics (see Figure 2.1).

1. Experiment analysis

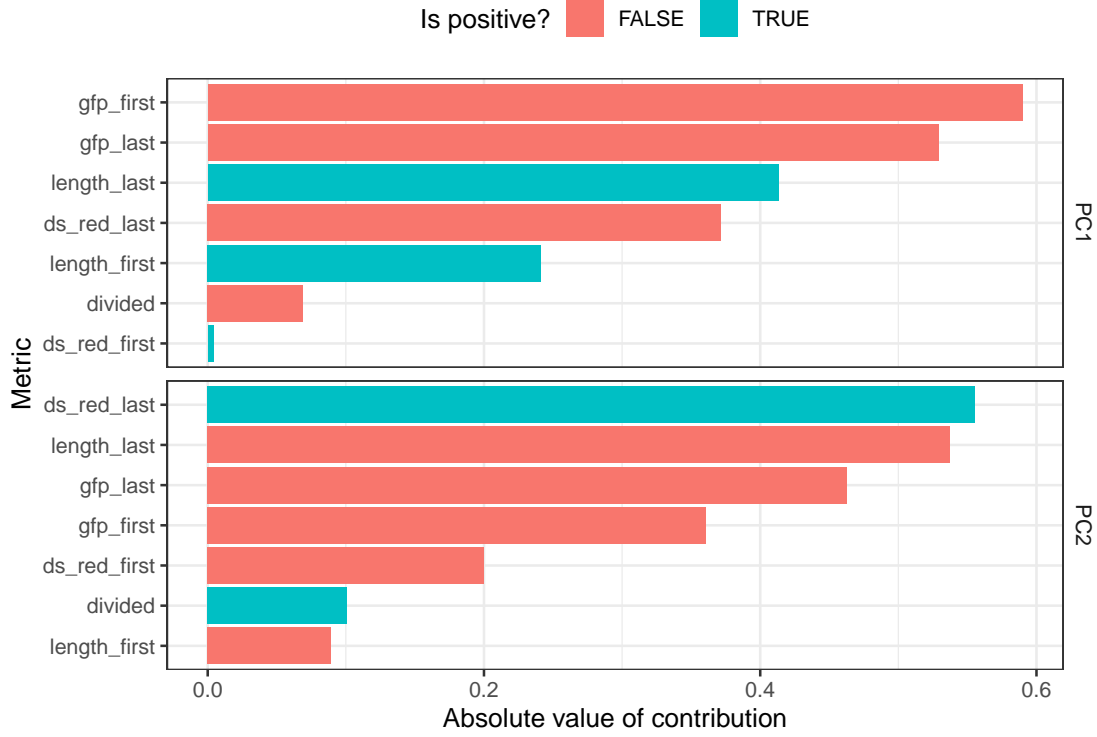


Figure 1.8: Variables contribution of Principal Component Analysis of chromosomal strain. In the figure 1.7, we see that the classes we created manually reflected what was observed when performing a reduction of dimensions analysis. The individual contribution of each variable for the first two components is shown here. The variables that most affected components 1 and 2 (X-axis and Y-axis, respectively) are the final measurements of DS-red, GFP, length, and the initial amount of GFP. Given that they are chromosomal strains, we should note that this variability could be produced by intrinsic experimental noise that we could not remove. With that in mind, having the DS-red and the final length highlights the inherent role of cells by having increased its size.

1. Experiment analysis

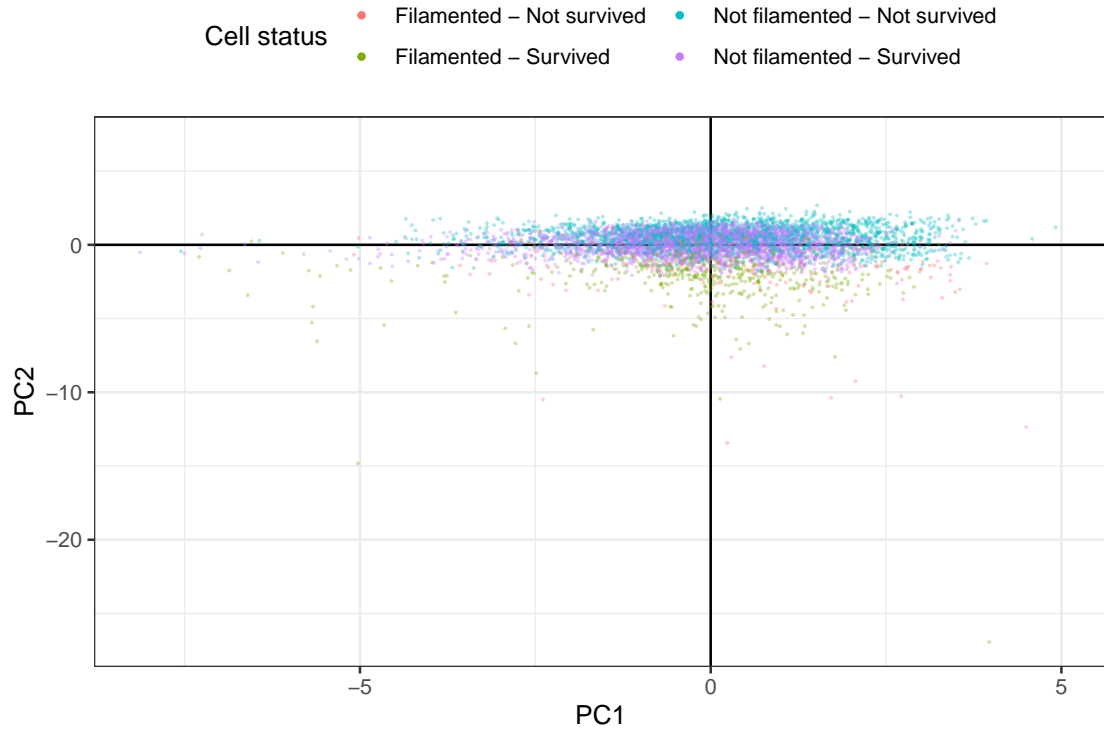


Figure 1.9: Principal Component Analysis of plasmid strain. By integrating the information from different variables in a dimensionality reduction analysis, we observed a clear separation between the filamented and non-filamented cells. Said class separation is given by component 2 (Y-axis), which is determined primarily by the initial and final lengths of the cells (see Figure 1.10). Furthermore, the classification also allows us to separate those filamented cells that died from those that survived. Therefore, despite the increase in the complexity of the system, length continues to play a role in determining survival.

1. Experiment analysis

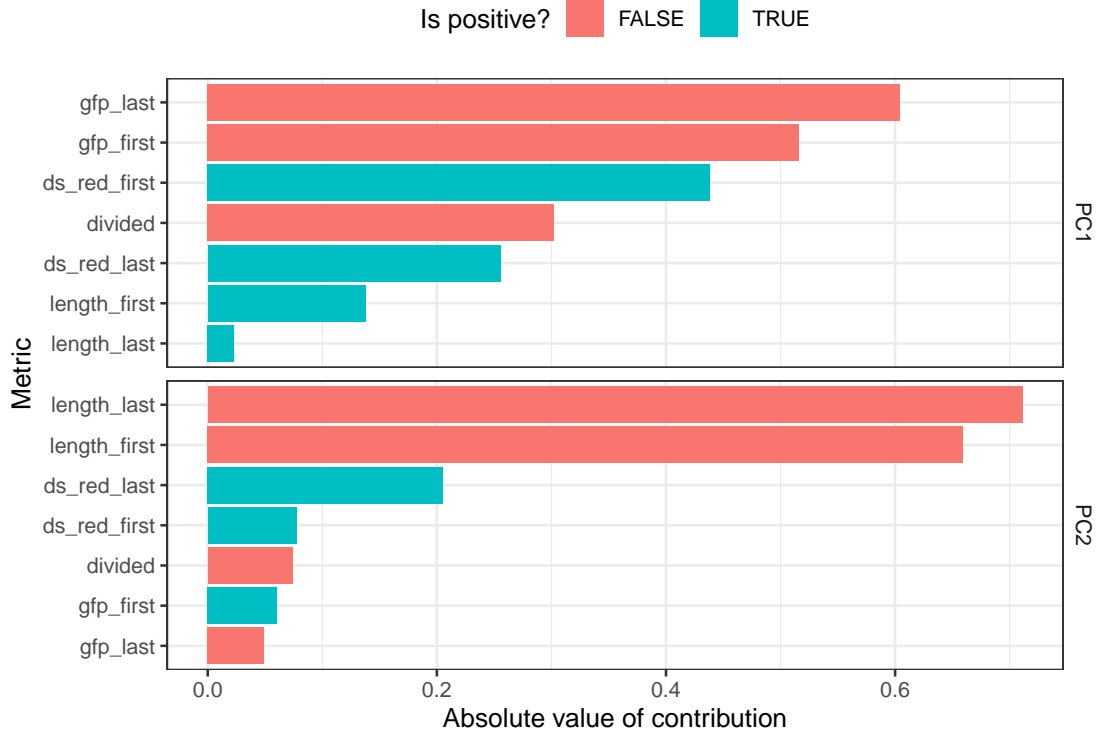


Figure 1.10: Variables contribution of Principal Component Analysis of plasmid strain. In Figure 1.9, we saw that we could separate the filamented cells from the non-filamented ones. The reduction analysis also shows a slight difference between surviving and dead cells within the small group of filamented cells. Here we offer the individual contribution of each variable for the first two components. For the first component (x-axis in Figure 1.7), the initial and final GFP measurements received mainly the variability. We expected this component's importance since, being a chromosomal strain, we hope that its inherent variation will be inherited into the system. On the other hand, the second component (Y-axis in Figure 1.7) was determined by the length of the cell. Factors that, in the chromosomal strain (see Figure 1.8), determined with the help of DS-red the separation between surviving and dead cells.

1. Experiment analysis

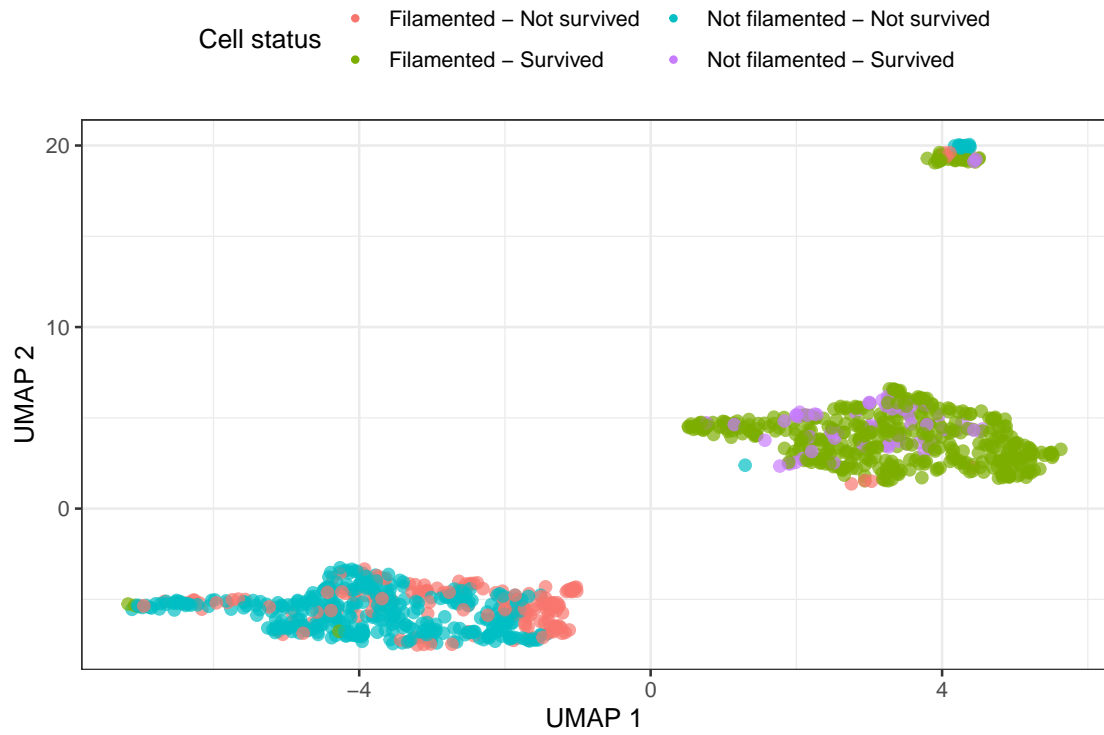


Figure 1.11: UMAP coordinates of chromosome strain. We represented the cells in a low dimensional space. This new projection made it possible to group the cells that survived and those that did not. Therefore, as in PCA Figure 1.7, this technique supports the manual classification that we perform. However, the distance between the groups has no real meaning.

1. Experiment analysis

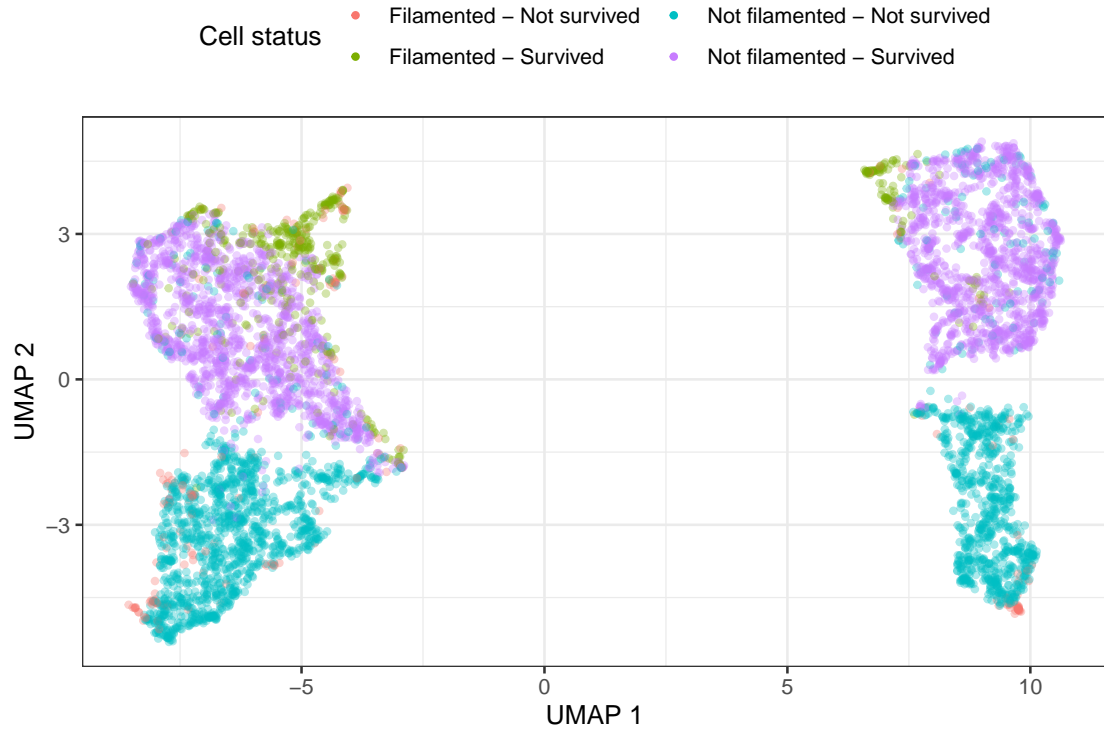


Figure 1.12: UMAP coordinates of plasmid strain. As in its 1.11 pair, the representation in a low-dimensional space helped classify the cells, grouping mainly into 4 groups, 2 of survivors and 2 of non-survivors. The variable “*division*” marks the separation of classes. The *division* variable indicates whether a cell divided during its lifetime or not. Together, the UMAP represents the manually assigned classes. The distance between the groups has no real meaning.

1. Experiment analysis

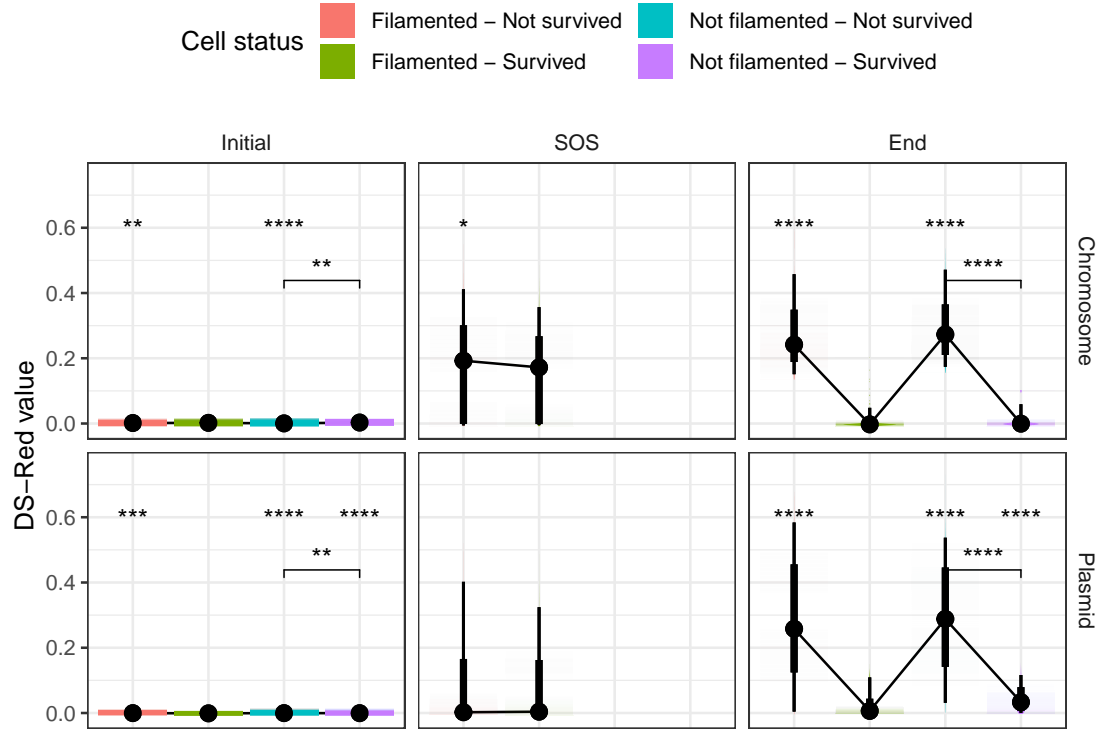


Figure 1.13: DS-red temporal distribution. To evaluate the incident effect of the antibiotic marked by DS-red on cells by class, we show its values at three key moments: start, filamentation (SOS), and end. The upper asterisks represent the significance value when comparing a group X to the filamented and surviving cell reference. Asterisks in a line indicate whether or not there is a significant difference in the survival of non-filamented cells. The black dots represent the mean of each group, and the lines that join them are a comparative guide. The extent of the black bars represents the distribution of the data. Although, at the initial time, we observe multiple significant differences, this is likely due to the intrinsic noise of the system since, as expected, the values are close to zero. We observed a difference between the surviving and non-filamented cells for the chromosomal strain for the SOS time, but the same did not occur for the plasmid strain. The final amount of DS-red makes a clear difference between survival and death.

1. Experiment analysis

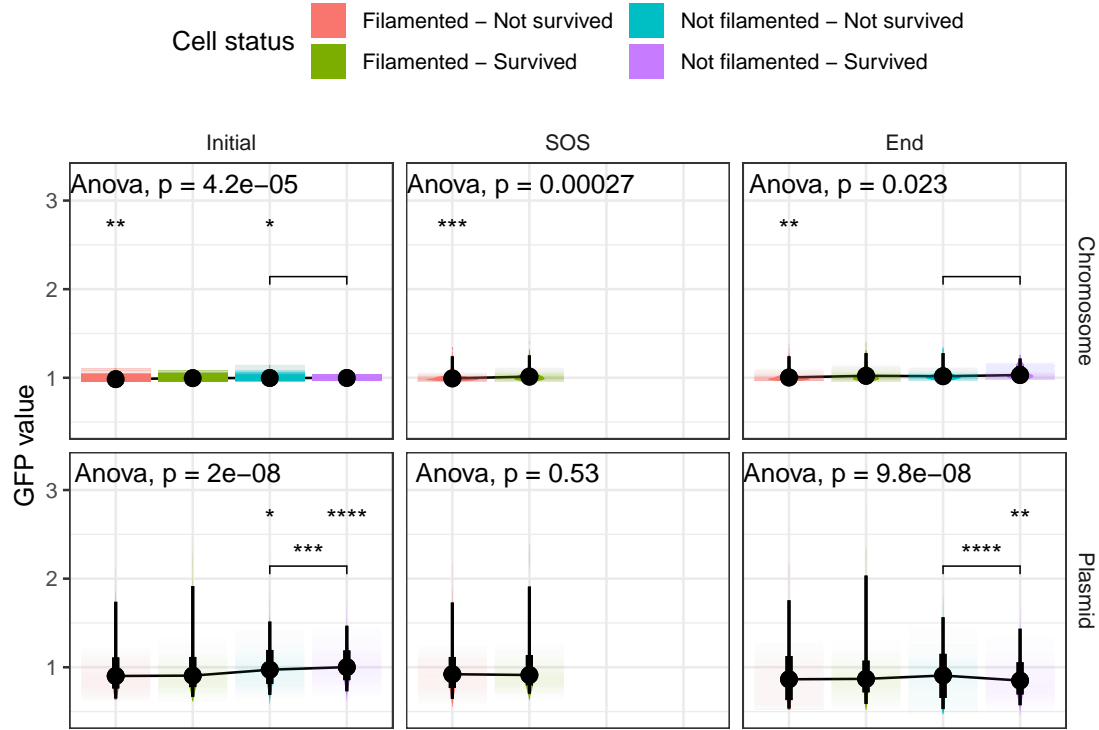


Figure 1.14: GFP temporal distribution. To evaluate the incident effect of the GFP on cells by class we used the same notation as in Figure 1.13. The chromosomal strain has significant values of GFP at different times. However, these differences can be mainly due to experimental noise. We appreciated in the plasmid strain that the filamented cells had a lower amount of initial GFP as expected. At the time of filamentation, there is no difference between the survivors and the dead. However, in the end time, we observed that the surviving non-filamented cells have less GFP than the dead non-filamented and the living filamented cells.

1. Experiment analysis

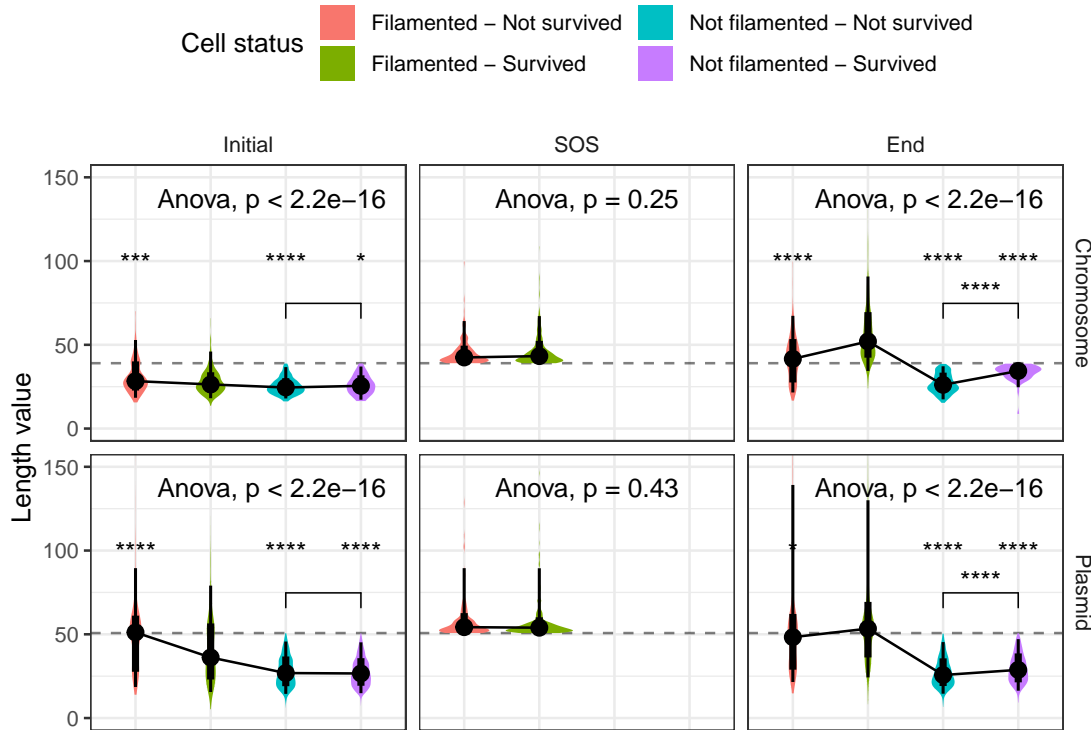


Figure 1.15: Length temporal distribution.

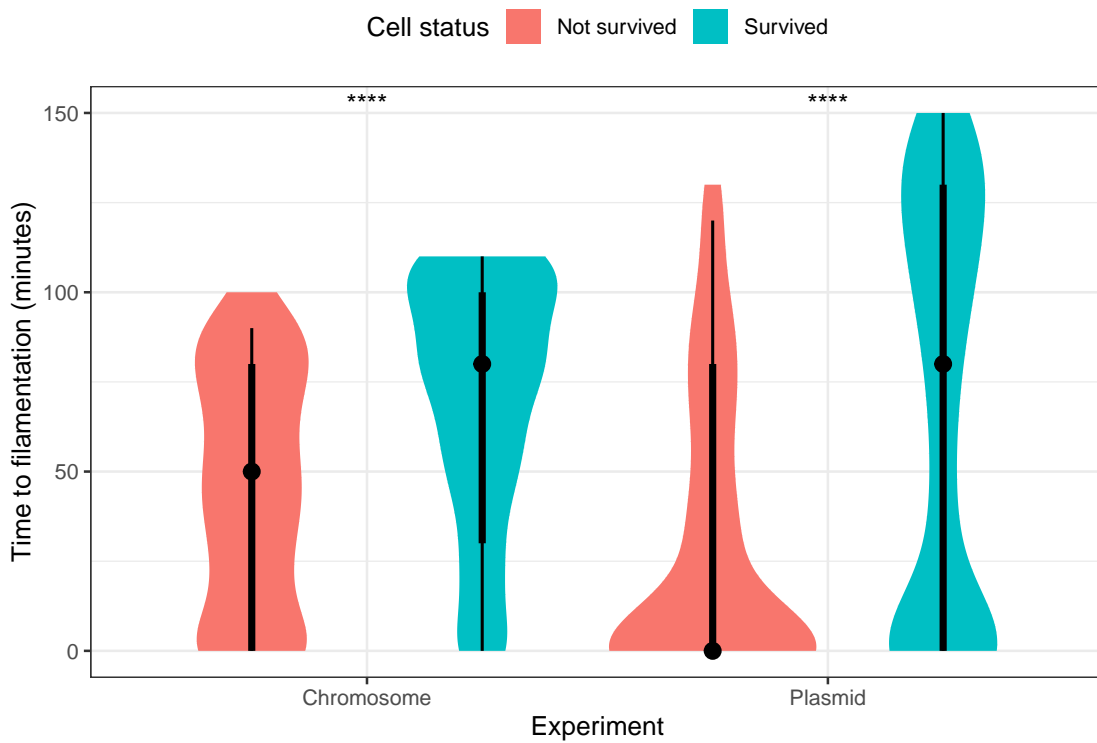


Figure 1.16: Time to filamentation without filters.

1. Experiment analysis

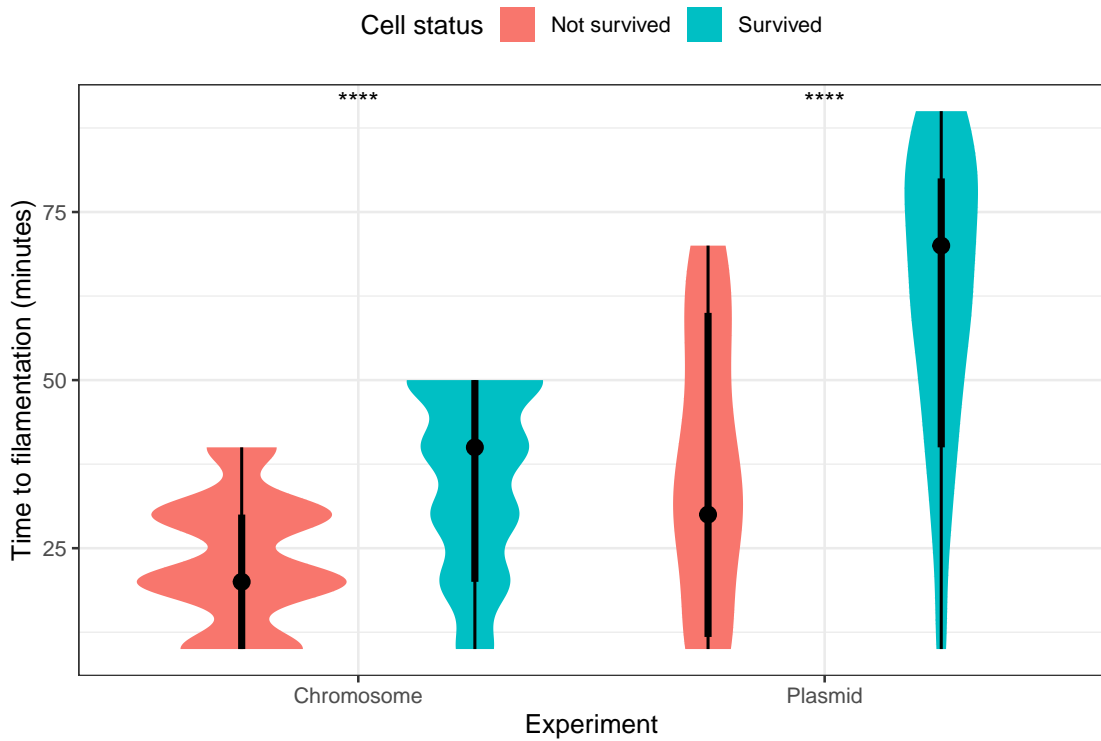


Figure 1.17: Time to filamentation filtered.

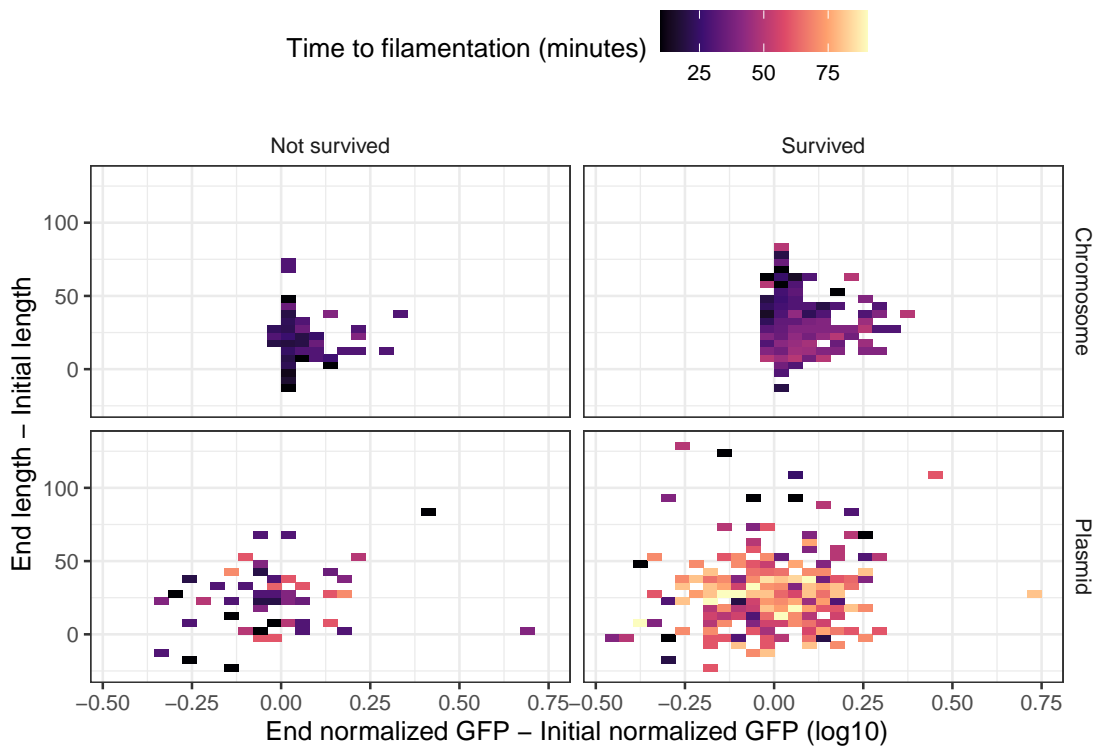


Figure 1.18: Experiment initial values differences with time.

1. Experiment analysis

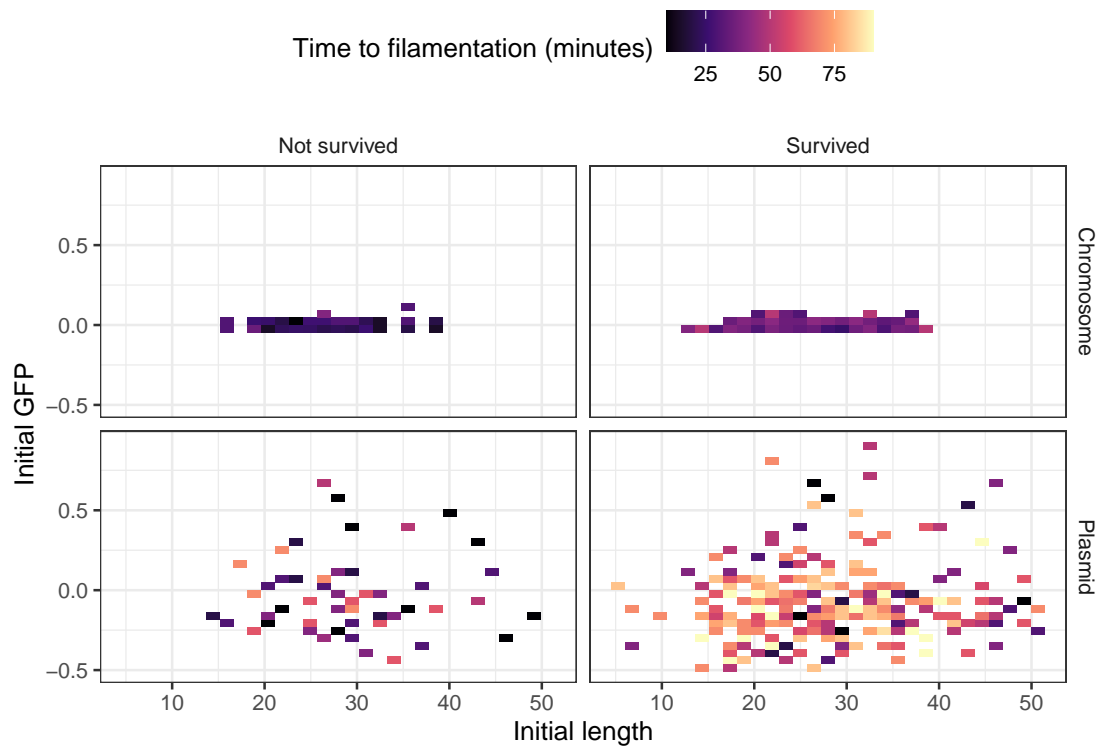


Figure 1.19: Experiment initial values with time.

1. Experiment analysis

1.3.3 Tracks level

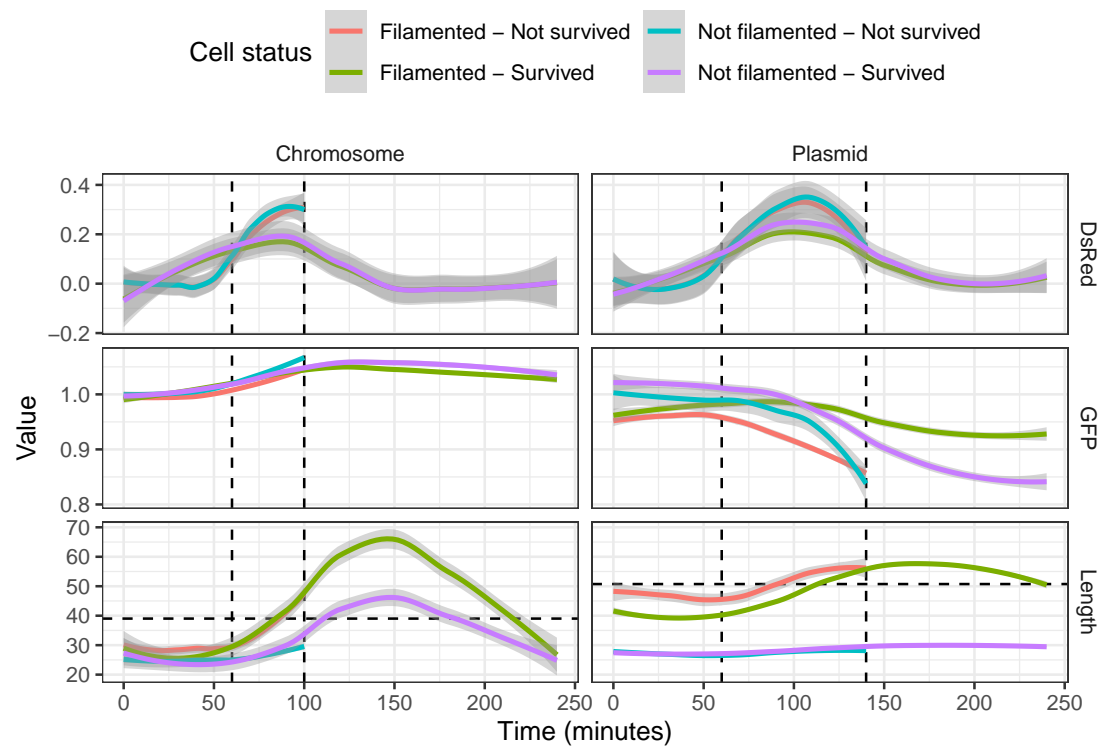


Figure 1.20: Population measurements over time.

1. Experiment analysis

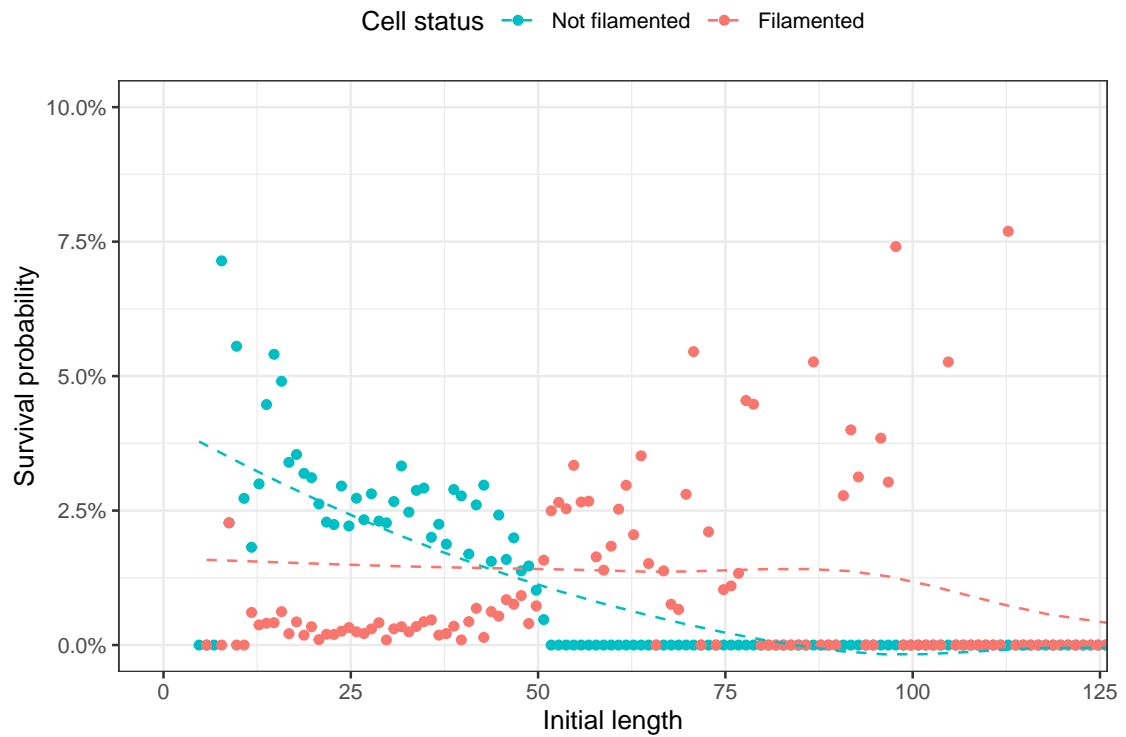


Figure 1.21: Plasmid initial GFP survival probability.

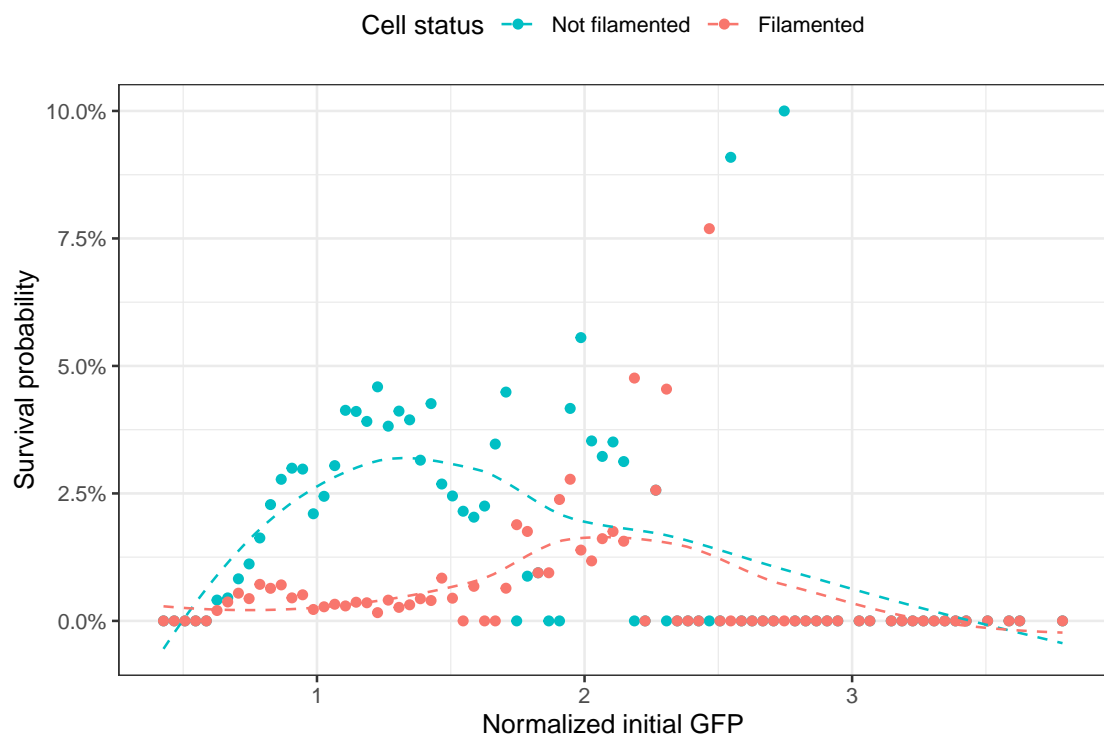


Figure 1.22: Plasmid initial length survival probability.

1. Experiment analysis

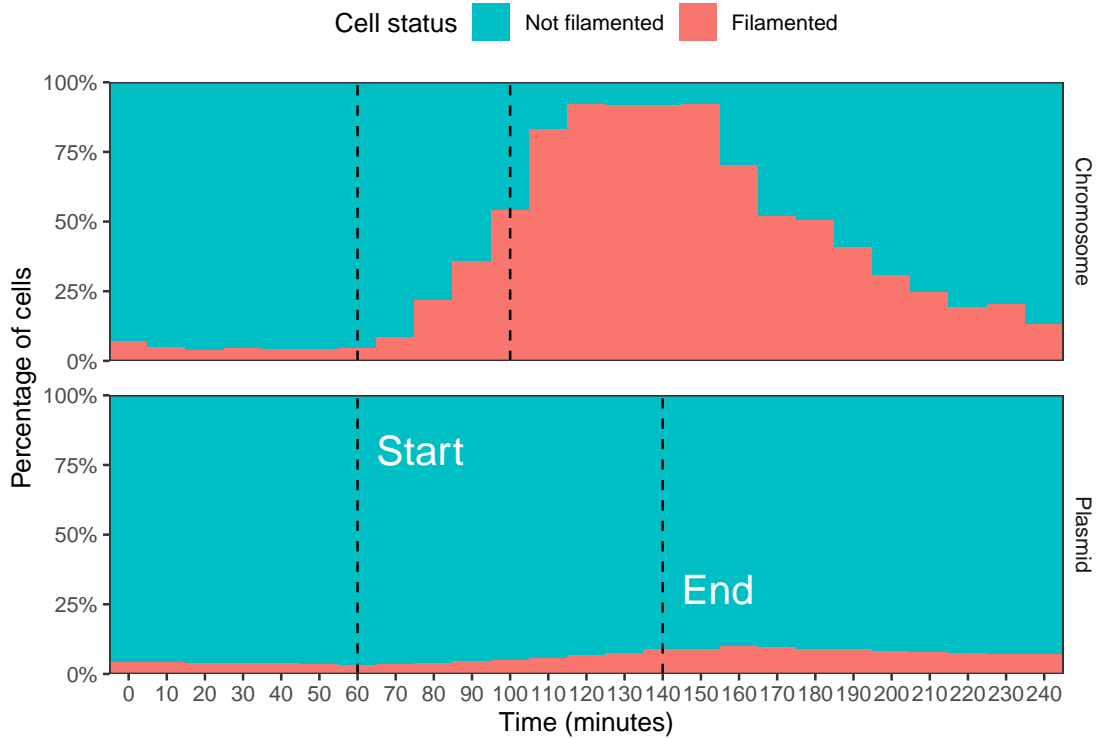


Figure 1.23: Population status over time without dead.

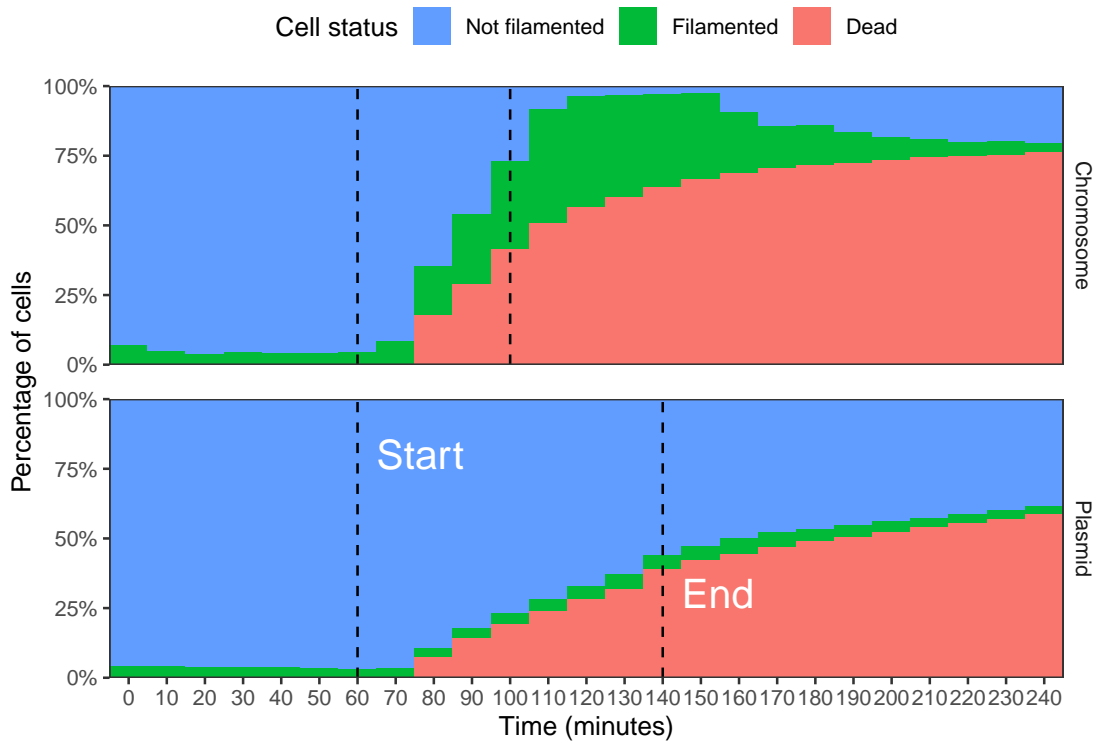


Figure 1.24: Population status over time with dead.

1. Experiment analysis

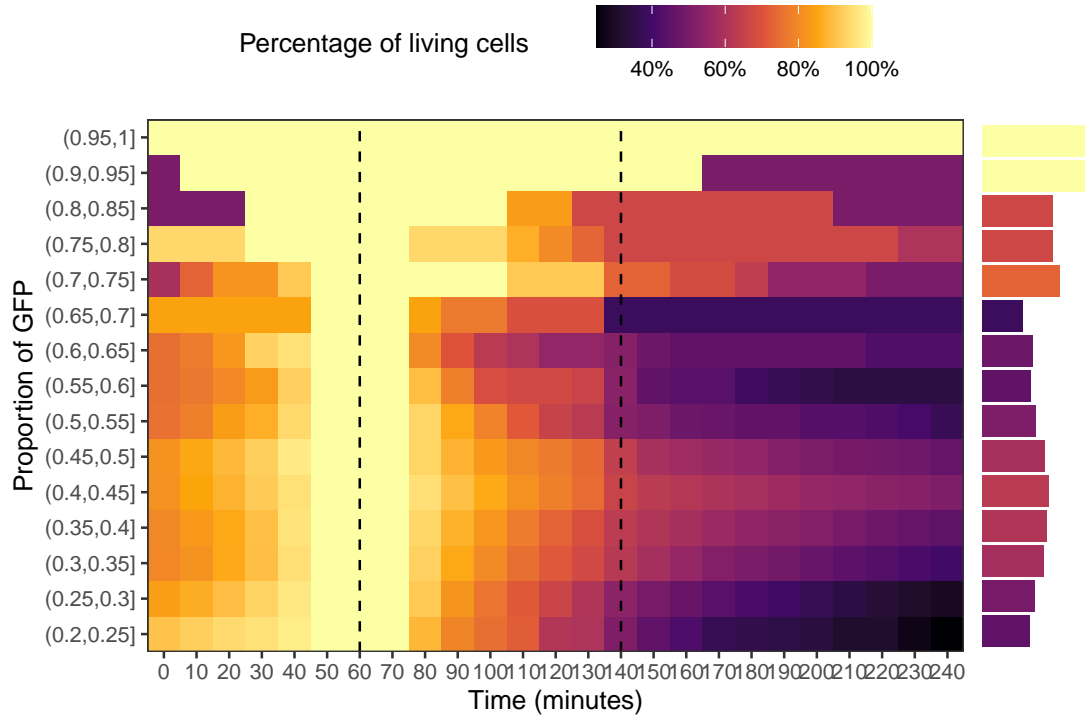


Figure 1.25: Population survivals binned by initial GFP over time.

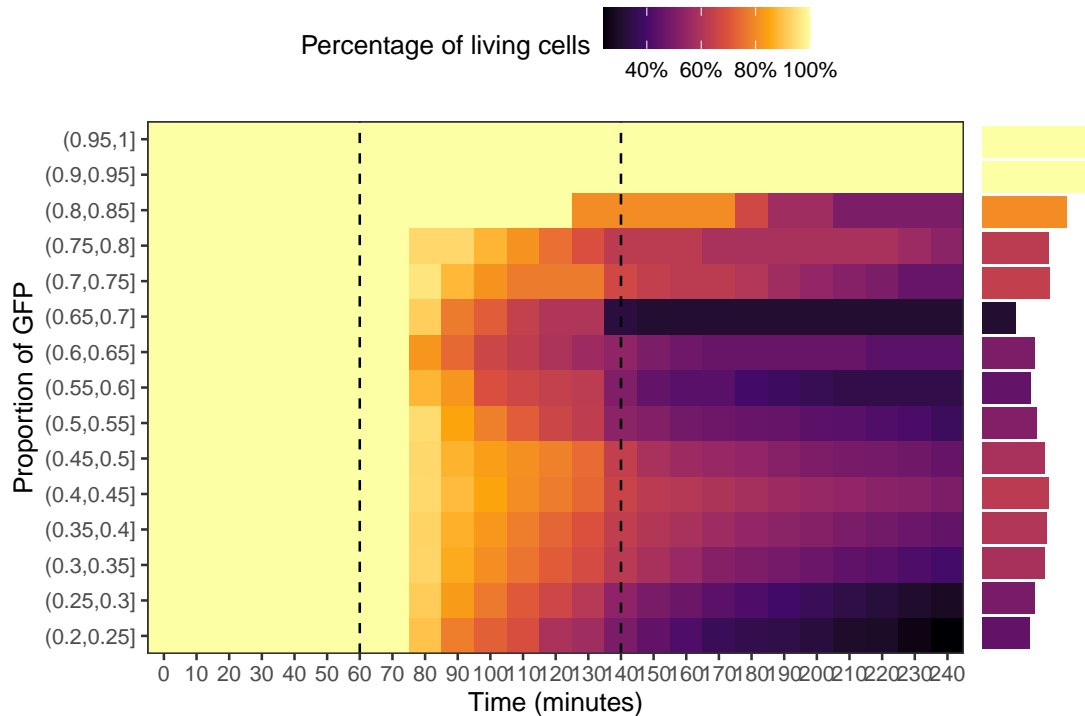


Figure 1.26: Normalized population survivals binned by initial GFP over time.

1. Experiment analysis

1.4 Discussion

2

Models to the rescue; filamentation abstraction

Contents

2.1	Introduction	27
2.2	Filamentation model	28
2.3	Results	29
2.3.1	Filamentation provides transient resistance under stressful conditions	29
2.3.2	Filamentation increases the minimum inhibitory concentration	31
2.3.3	Heterogeneity in the toxin-antitoxin system represents a double-edged sword in survival probability	32
2.4	Discussion	35

Scientists have extensively studied the mechanisms that orchestrate the growth and division of bacterial cells. Cells adapt their shape and dimensions in response to variations in the intracellular and extracellular environments by integrating information about the presence of nutrients or harmful agents in the decision to grow or divide. Filamentation is a process that occurs when rod-shaped cells stop dividing but continue to grow, thus producing elongated cells. Some cells can naturally grow as filamentous, while others only do so under stressful conditions. Here we use mathematical modeling and computational simulations to evaluate

2. Models to the rescue; filamentation abstraction

a toxic agent's intracellular concentration as a function of cell length. We show that filamentation can act as a strategy that promotes the resilience of a bacterial population under stressful environmental conditions.

2.1 Introduction

By integrating information from the environment, cells can alter their cell cycle. For instance, some cells arrest the cell division in the presence of toxic agents but continue to grow. Previous studies have shown that this filamentation phenomenon provides a mechanism that enables cells to cope with stress, which leads to an increase in the probability of survival (Justice, Hunstad, Cegelski, et al. 2008). For example, filamentation can be a process capable of subverting innate defenses during urinary tract infection, facilitating the transition of additional rounds of intracellular bacterial community formation (Justice, Hunstad, Seed, et al. 2006).

Although filament growth can help mitigate environmental stress (e.g., by activating the SOS response system (Justice, Hunstad, Cegelski, et al. 2008)), the evolutionary benefits of producing elongated cells that do not divide are unclear. Here, we proposed a mathematical model based on ordinary differential equations that explicitly considers the concentration of intracellular toxin as a function of the cell's length (see Equation (2.1)). The model is built based on the growth ratio of measurements of the surface area (SA) and the cell volume (V), whereby the uptake rate of the toxin depends on the SA . However, V 's rate of change for SA is higher than SA for V , which results in a transient reduction in the intracellular toxin concentration (see Figure 2.1). Therefore, we hypothesized that this geometric interpretation of filamentation represents a biophysical defense line to increase the probability of a bacterial population's survival in response to stressful environments.

2. Models to the rescue; filamentation abstraction

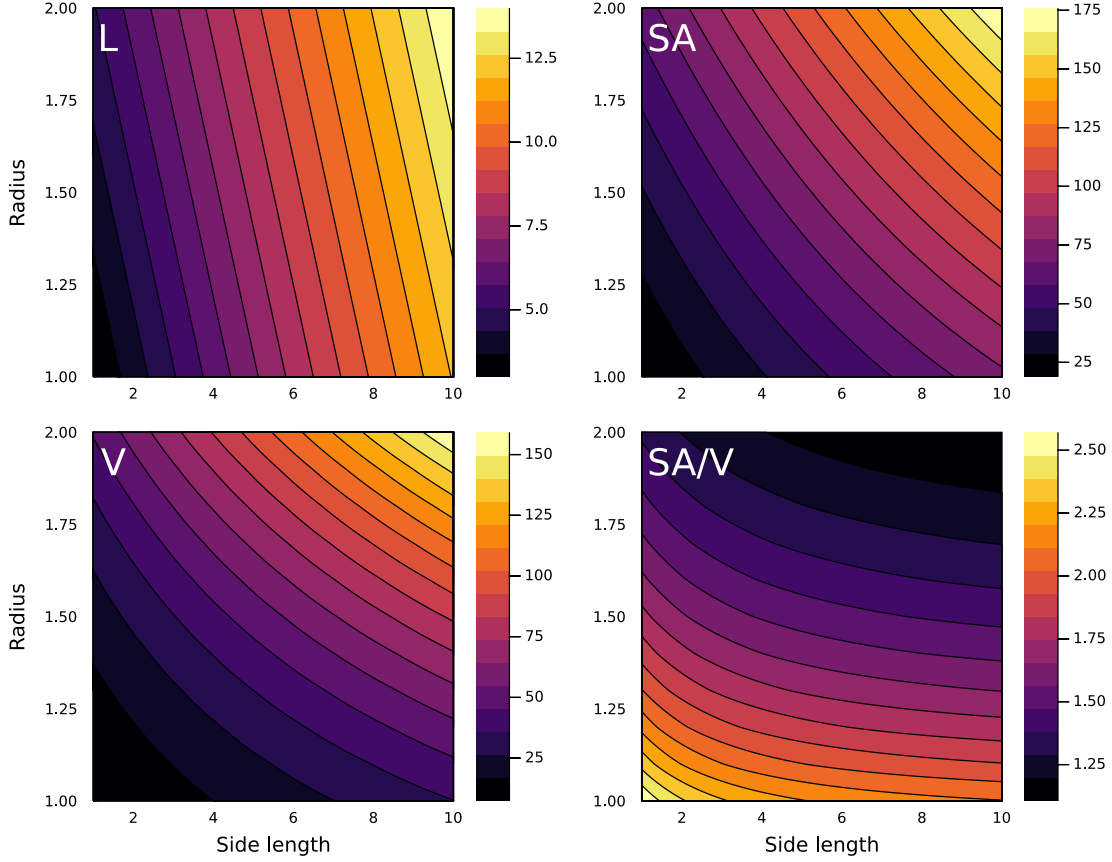


Figure 2.1: Cell dimensions relationship. We evaluated the resulting geometric properties on a grid of side lengths and radii with a pill-shaped cell. We can see that by maintaining a constant radius (typical case in bacteria such as *E. coli*) and increasing the side length, the surface area / volume relationship (SA/V) tends to decline since the V will grow at a higher rate than the SA .

2.2 Filamentation model

Let us assume the shape of cells is a cylinder with hemispherical ends. Based on this geometric structure, a nonlinear system of differential equations governing filamentation can be written as follows:

$$\begin{aligned} \frac{dT_{int}}{dt} &= T_{sa} \cdot (T_{ext}(t) - T_{vol}) - \alpha \cdot T_{ant} \cdot T_{int} \\ \frac{dL}{dt} &= \begin{cases} \beta \cdot L, & \text{if } T_{int} \geq T_{sos}, t \geq \tau_{sos} + \tau_{delay} \text{ and } L < L_{max} \\ 0, & \text{otherwise} \end{cases} \end{aligned} \quad (2.1)$$

It considers the internal toxin (T_{int}) and the cell length (L) as variables. T_{sa} and T_{vol} represent the surface area and volume of the toxin in the cell, respectively.

2. Models to the rescue; filamentation abstraction

$T_{ext}(t)$ is a function that returns the amount of toxin in the cell medium. T_{anti} and α symbolize the amount of antitoxin and its efficiency rate, respectively. β as the rate of filamentation. L_{max} is the maximum size that the cell can reach when filamentation is on. T_{sos} and T_{kill} are thresholds for filamentation and death, respectively. Finally, τ_{delay} is the amount of time required to activate filamentation after reaching the T_{sos} threshold.

2.3 Results

2.3.1 Filamentation provides transient resistance under stressful conditions

When growing rod-shaped bacterial cells under constant conditions, the distribution of lengths and radii is narrow (Schaechter, Williamson, et al. 1962). However, when growing under stress conditions, some cells produce filaments (Schaechter, MaalOe, et al. 1958). This phenomenon may depend on the SOS response system (Bos et al. 2015), which can repair DNA damage, giving the cell greater chances of recovering and surviving under stress conditions. Besides, the SOS response has been reported to have precise temporal coordination in individual bacteria (Friedman et al. 2005). Among the stress conditions that can trigger the SOS response is exposure to beta-lactam antibiotics (Miller 2004).

In general, filamentation has been studied as an unavoidable consequence of stress. However, we considered filamentation an active process that produces the first line of defense against toxic agents. Therefore, a differential equation model was proposed that assesses the change in the amount of internal toxin as a function of cell length. At the core of this model, we include the intrinsic relationship between the surface area and the capsule volume since it is vital in determining cell size (Harris and Theriot 2016).

In figure 2.2, cells grow in a ramp-shaped external toxin signal without considering a toxin-antitoxin system. As time progresses, the toxin in the external environment increases, so the cell raises its internal toxin levels. At approximately

2. Models to the rescue; filamentation abstraction

time 22, any cell reaches T_{sos} . The control cell (unable to filament) and the average cell (capable of filamenting) reach the death threshold, T_{kill} , at times 31 and 93 (hatched and solid black lines), respectively. Therefore, under this example, the cell has increased its life span three times more than in control by growing as a filament (green shaded area versus orange shaded area). In turn, figure 2.2 also shows stochastic simulations of the system in the intake of internal toxins. Considering that cell growth and death processes are inherently stochastic, stochastic simulations would be a better approximation. However, from now on, we will continue with the study of the deterministic model.

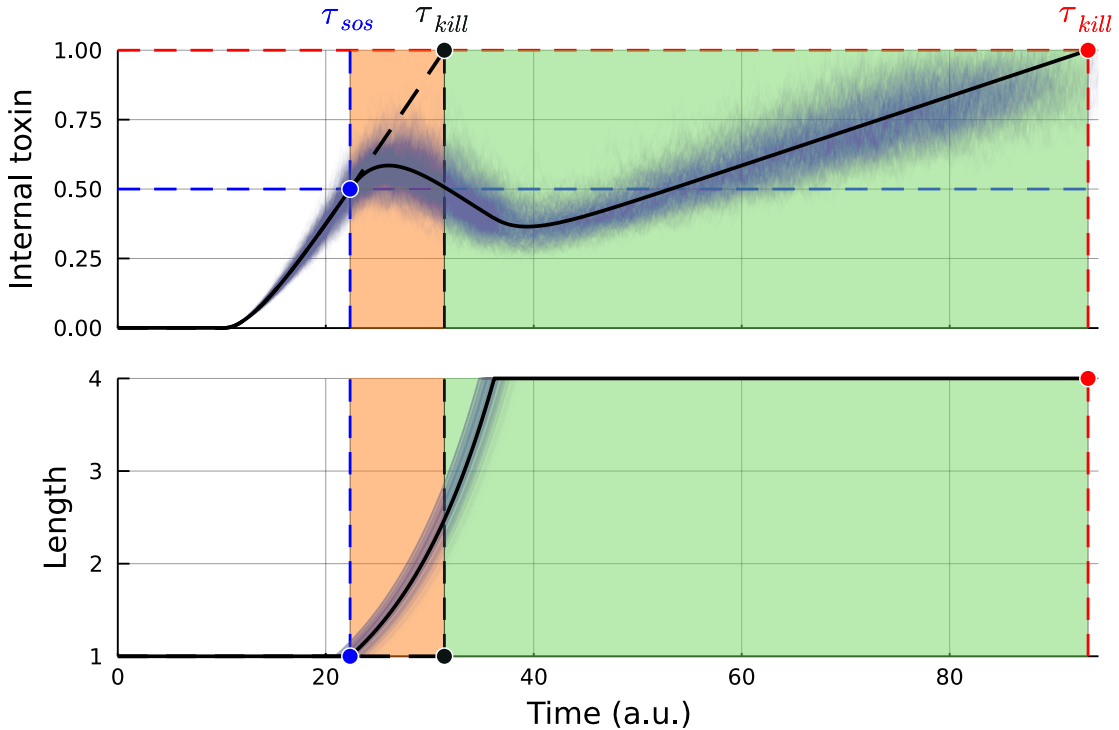


Figure 2.2: Effect of filamentation on intracellular toxin concentration. In the presence of an extracellular toxic agent, the intracellular concentration of the toxin (T_{int}) increases until reaching a damage threshold that triggers filamentation (T_{sos} , blue point), increasing cell length (L). When filamentation is on, the cell decreases T_{int} due to the intrinsic relationship between surface area and cell volume. When the cell reaches its maximum length, it eventually dies if the stressful stimulus is not removed (T_{kill} , red dot). The hatched line represents a cell that can not grow as filament. The orange shaded area is the time between stress and the non-filament cell's death, while the green shaded area represents the temporal gain for doing so. The blue background lines represent stochastic simulations of the same system.

2. Models to the rescue; filamentation abstraction

2.3.2 Filamentation increases the minimum inhibitory concentration

Antimicrobial resistance (AMR) can be considered one of the most critical health problems of the century. That is, microorganisms' ability to grow despite exposure to substances designed to inhibit their growth or kill them. In April 2014, the World Health Organization (WHO) published its first global report on AMR surveillance (“Editorial Board” 2014). Taking out of the darkness a common fear, a possible post-antibiotic future in which common infections or minor injuries can kill. Therefore, understanding the mechanisms of avoiding antibiotic action is essential for producing knowledge and developing strategies that reduce the generation of resistant bacteria.

A classic experiment in laboratories finds the concentration that inhibits bacterial growth through exposure to different toxin doses. The concentration found is known as the minimum inhibitory concentration (MIC) (Andrews 2002). Bacteria are capable of modifying their MIC through various mechanisms, for example, mutations (Lambert 2005), impaired membrane permeability (Sato and Nakae 1991), flux pumps (Webber 2003), toxin-inactivating enzymes (Wright 2005), and plasticity phenotypic (Justice, Hunstad, Cegelski, et al. 2008). The latter is our phenomenon of interest because it considers the change in shape and size, allowing us to study it as a strategy to promote bacterial survival.

We decided to analyze the MIC change caused by filamentation through stable exposure experiments of different toxin amounts at other exposure times. Computational simulations show that when comparing cells unable to filament with those that can, there is an increase in the capacity to tolerate more generous amounts of toxin, increasing their MIC (see Figure 2.3). Therefore, it confers a gradual increase in resistance beyond filamentation's role in improving the cell's life span as the exposure time is longer.

2. Models to the rescue; filamentation abstraction

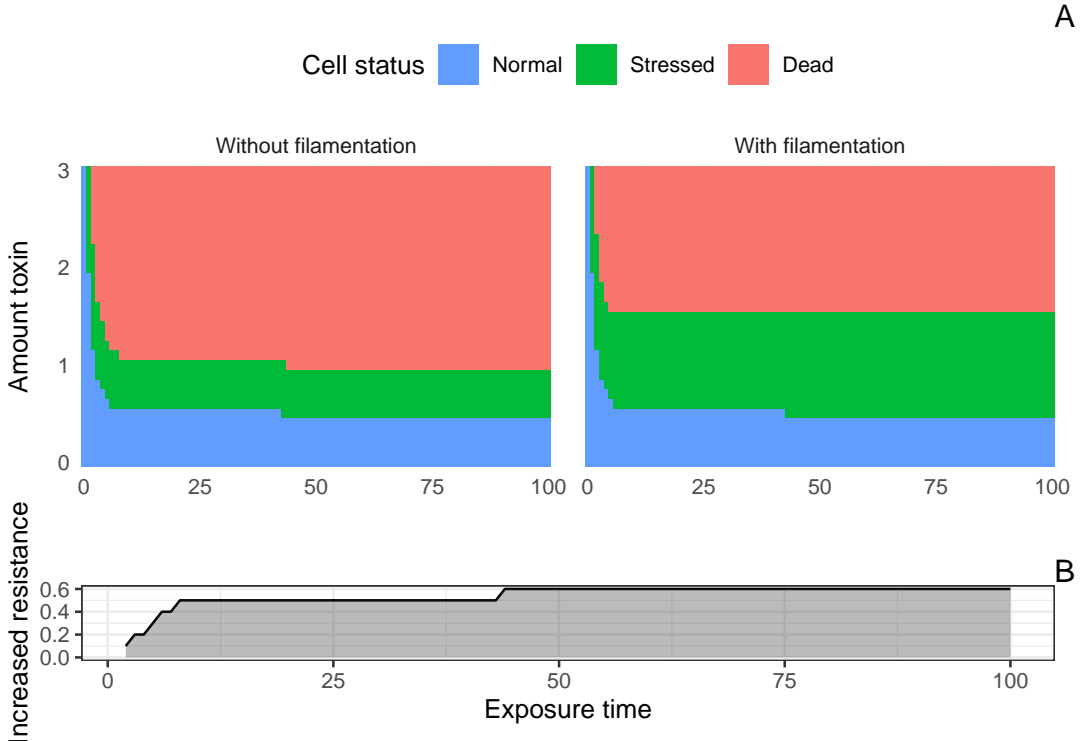


Figure 2.3: Effect of filamentation on minimum inhibitory concentration (MIC). By exposing a cell to different toxin concentrations with stable signals, the cell achieves a set MIC for conditions without or with filamentation (separation between stressed and dead state) for each exposure time, without representing a change for the normal state cells' points (blue zone). Thus, the green line represents a gradual MIC increase when comparing each MIC between conditions for each exposure time.

2.3.3 Heterogeneity in the toxin-antitoxin system represents a double-edged sword in survival probability

One of the SOS response system properties is that it presents synchronous activation times within homogeneous populations (Friedman et al. 2005). It has constant gene expression rates that help it cope with stress; however, it is possible to introduce variability by considering having multicopy resistance plasmids (Million-Weaver and Camps 2014). Therefore, the response times would have an asynchronous behavior at the global level but synchronous at the local level.

To include this observation into the model, we include a negative term to the internal toxin representing a toxin-antitoxin system. Therefore, the model now has an efficiency rate of the antitoxin and a stable amount per cell. We simulate

2. Models to the rescue; filamentation abstraction

the effect of the toxin-antitoxin system variation within a 1000 cell population; we initialize each one with similar initial conditions, except for the amount of internal antitoxin, defined as $T_{anti} \sim N(\mu, \sigma)$. Considering that T_{anti} values < 0 are equal to 0. For each experiment, $\mu = 25$, while it was evaluated in the range $[0 - 20]$. For the generation of pseudo-random numbers and to ensure the results' reproducibility, the number 42 was considered seed.

As shown in Figure 2.4, when we compare heterogeneous populations in their toxin-antitoxin system, we can achieve different population dynamics, that is, changes in the final proportions of cell states; normal, stressed, and dead. This difference is because the cell sometimes has more or less antitoxin to handle the incoming stress situation.

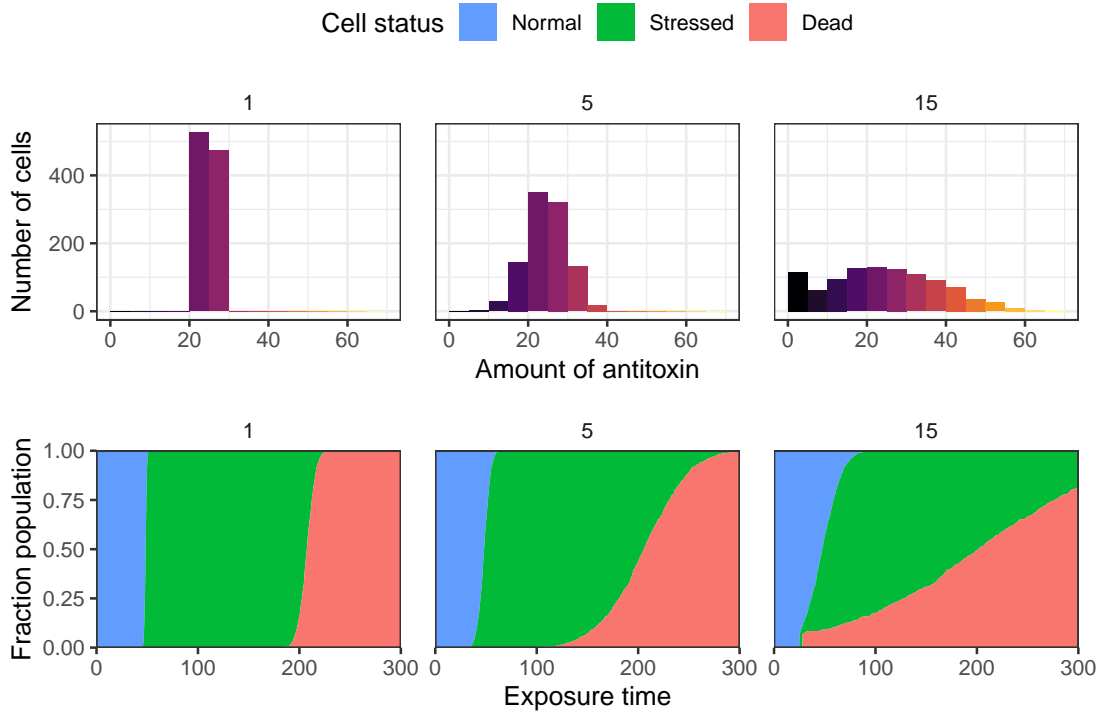


Figure 2.4: Variability in the toxin-antitoxin system produces different proportions of cell states. Histograms represent the distribution of antitoxin quantity, while the curves represent the population's fraction over time. The cell will start to filament after reaching a certain internal toxin threshold, T_{sos} . Therefore, the expected global effect on the population's response times based on the amount of antitoxin is asynchronous, while at the local level, it is synchronous. Consequently, different proportions are presented in the cellular states since some cells will activate the filamentation system before and others later.

2. Models to the rescue; filamentation abstraction

Considering that the toxin-antitoxin system's variability can modify the proportions of final cell states, a question arose about heterogeneity levels' global behavior. To answer this question, we evaluate the probability of survival for each population, defined by its distribution of antitoxin levels. In this way, we characterized the population survival probability function into three essential points according to its effect: negative, invariant, and positive (see Figure 2.5). Furthermore, these points are relative to the homogeneous population's death time in question (τ_{kill}): when $t < \tau_{kill}$ will represent a detrimental effect on survival, $t = \tau_{kill}$ will be independent of variability, and $t > \tau_{kill}$ will be a beneficial point for survival. Therefore, we concluded that the effect of heterogeneity in a toxin-antitoxin system represents a double-edged sword.

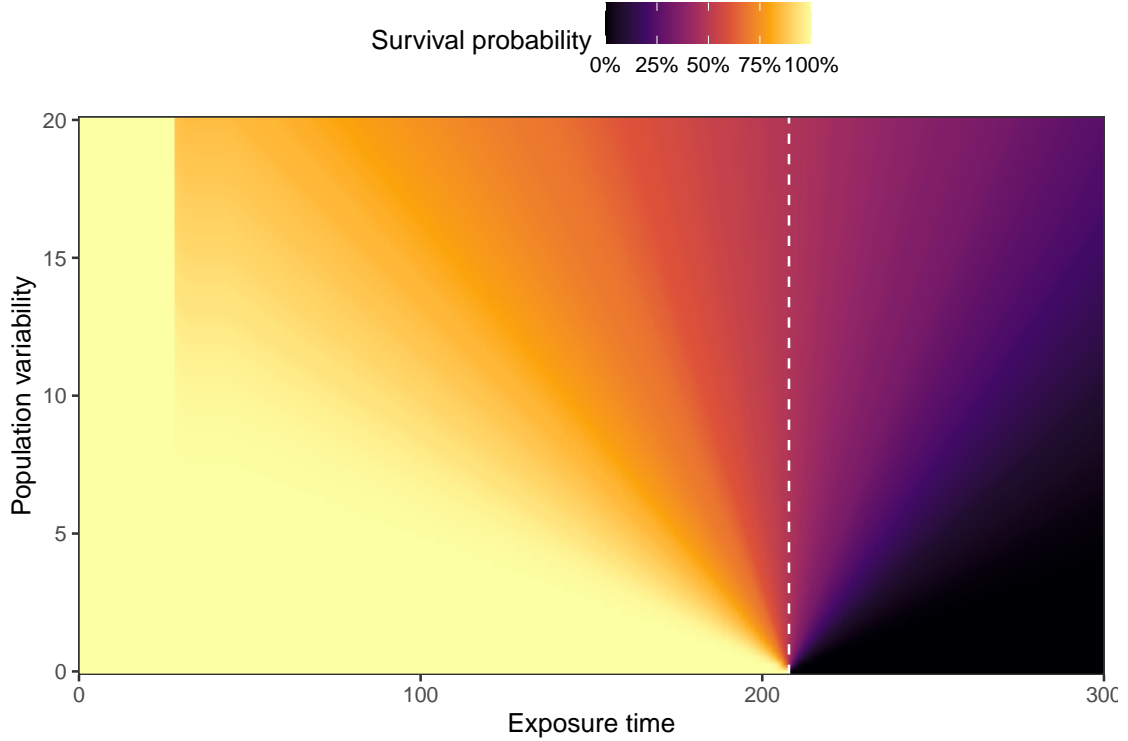


Figure 2.5: Effect of variability on the toxin-antitoxin system. The color of the heatmap is representative of the fraction of living cells at exposure time. The white vertical line represents the death time of the homogeneous population (τ_{kill}). At $t < \tau_{kill}$, it is shown that the fraction of survivors decreases as the variability in the population increases. When $t = \tau_{kill}$, the variability does not affect the fraction of survivors, but it represents a percentage improvement for the homogeneous population. Finally, when $t > \tau_{kill}$, the heterogeneity of the population favors survival.

2. Models to the rescue; filamentation abstraction

2.4 Discussion

Today, there have been advancements in the number of techniques that have allowed it to extend quantitative analyses to individual cells' dynamic observations (Campos et al. 2014; Meldrum 2005; Sliusarenko et al. 2011; Taheri-Araghi et al. 2017; Ursell et al. 2017). Therefore, studying their cellular behavior every day from medium to medium can be somewhat reproducible, facilitating the association of complex biological functions in simple mathematical equations (Neidhardt 1999).

Here, we proposed a mathematical model showing that filamentation could serve as a population's resilience mechanism to stress conditions. Finding that filamentation's net effect generates an additional window of time for the cell to survive, decreasing the toxin's intracellular concentration. However, we also found that a side effect of filamentation is to increase the cell's minimum inhibitory concentration. On the other hand, when we introduce variability in the amount of antitoxin in a cell population, we found that heterogeneity can be a double-edged sword, sometimes detrimental and sometimes beneficial, depending on the time of exposure to the toxic agent.

Due to the above, despite being simple, the model could have the ability to recapitulate the behavior seen in nature from variables that we can calculate easily with single-cell measurements. However, in other situations, it could be helpful to consider the addition of variables such as cell wall production and peptidoglycans' accumulation, among others. Notwithstanding the lack of parameters that are a little closer to reality, confirming that the model can work under experimental conditions would represent an achievement due to its explanatory simplicity, starting, in this way, the path of the study of filamentation oriented to the ecology of stress.

3

Discussion

Appendices

A

The First Appendix

Works Cited

- Andrews, J. M. (June 2002). "Determination of Minimum Inhibitory Concentrations". In: *Journal of Antimicrobial Chemotherapy* 49.6, pp. 1049–1049. DOI: [10.1093/jac/dkf083](https://doi.org/10.1093/jac/dkf083).
- Bos, Julia et al. (Jan. 2015). "Emergence of Antibiotic Resistance from Multinucleated Bacterial Filaments". en. In: *Proceedings of the National Academy of Sciences* 112.1, pp. 178–183. DOI: [10.1073/pnas.1420702111](https://doi.org/10.1073/pnas.1420702111).
- Campos, Manuel et al. (Dec. 2014). "A Constant Size Extension Drives Bacterial Cell Size Homeostasis". en. In: *Cell* 159.6, pp. 1433–1446. DOI: [10.1016/j.cell.2014.11.022](https://doi.org/10.1016/j.cell.2014.11.022).
- "Editorial Board" (June 2014). en. In: *Journal of Global Antimicrobial Resistance* 2.2, p. ii. DOI: [10.1016/S2213-7165\(14\)00044-7](https://doi.org/10.1016/S2213-7165(14)00044-7).
- Friedman, Nir et al. (June 2005). "Precise Temporal Modulation in the Response of the SOS DNA Repair Network in Individual Bacteria". en. In: *PLoS Biology* 3.7. Ed. by Bénédicte Michel, e238. DOI: [10.1371/journal.pbio.0030238](https://doi.org/10.1371/journal.pbio.0030238).
- Harris, Leigh K. and Julie A. Theriot (June 2016). "Relative Rates of Surface and Volume Synthesis Set Bacterial Cell Size". en. In: *Cell* 165.6, pp. 1479–1492. DOI: [10.1016/j.cell.2016.05.045](https://doi.org/10.1016/j.cell.2016.05.045).
- Justice, S. S., D. A. Hunstad, P. C. Seed, et al. (Dec. 2006). "Filamentation by Escherichia Coli Subverts Innate Defenses during Urinary Tract Infection". en. In: *Proceedings of the National Academy of Sciences* 103.52, pp. 19884–19889. DOI: [10.1073/pnas.0606329104](https://doi.org/10.1073/pnas.0606329104).
- Justice, Sheryl S., David A. Hunstad, Lynette Cegelski, et al. (Feb. 2008). "Morphological Plasticity as a Bacterial Survival Strategy". en. In: *Nature Reviews Microbiology* 6.2, pp. 162–168. DOI: [10.1038/nrmicro1820](https://doi.org/10.1038/nrmicro1820).
- Lambert, P (July 2005). "Bacterial Resistance to Antibiotics: Modified Target Sites". en. In: *Advanced Drug Delivery Reviews* 57.10, pp. 1471–1485. DOI: [10.1016/j.addr.2005.04.003](https://doi.org/10.1016/j.addr.2005.04.003).
- Meldrum, Deirdre (Jan. 2005). *Faculty Opinions Recommendation of Bacterial Persistence as a Phenotypic Switch*. DOI: [10.3410/f.1021664.264823](https://doi.org/10.3410/f.1021664.264823).
- Miller, C. (Sept. 2004). "SOS Response Induction by -Lactams and Bacterial Defense Against Antibiotic Lethality". en. In: *Science* 305.5690, pp. 1629–1631. DOI: [10.1126/science.1101630](https://doi.org/10.1126/science.1101630).
- Million-Weaver, Samuel and Manel Camps (Sept. 2014). "Mechanisms of Plasmid Segregation: Have Multicopy Plasmids Been Overlooked?" en. In: *Plasmid* 75, pp. 27–36. DOI: [10.1016/j.plasmid.2014.07.002](https://doi.org/10.1016/j.plasmid.2014.07.002).
- Neidhardt, Frederick C. (Dec. 1999). "Bacterial Growth: Constant Obsession with dN/Dt ". en. In: *Journal of Bacteriology* 181.24, pp. 7405–7408. DOI: [10.1128/JB.181.24.7405-7408.1999](https://doi.org/10.1128/JB.181.24.7405-7408.1999).

Works Cited

- Sato, Kazuhito and Taiji Nakae (1991). "Outer Membrane Permeability of *Acinetobacter Calcoaceticus* and Its Implication in Antibiotic Resistance". en. In: *Journal of Antimicrobial Chemotherapy* 28.1, pp. 35–45. DOI: [10.1093/jac/28.1.35](https://doi.org/10.1093/jac/28.1.35).
- Schaechter, M., O. MaalOe, and N. O. Kjeldgaard (Dec. 1958). "Dependency on Medium and Temperature of Cell Size and Chemical Composition during Balanced Growth of *Salmonella Typhimurium*". en. In: *Journal of General Microbiology* 19.3, pp. 592–606. DOI: [10.1099/00221287-19-3-592](https://doi.org/10.1099/00221287-19-3-592).
- Schaechter, M., J. P. Williamson, et al. (Nov. 1962). "Growth, Cell and Nuclear Divisions in Some Bacteria". en. In: *Journal of General Microbiology* 29.3, pp. 421–434. DOI: [10.1099/00221287-29-3-421](https://doi.org/10.1099/00221287-29-3-421).
- Sliusarenko, Oleksi et al. (May 2011). "High-Throughput, Subpixel Precision Analysis of Bacterial Morphogenesis and Intracellular Spatio-Temporal Dynamics: Quantitative Analysis of Spatio-Temporal Dynamics". en. In: *Molecular Microbiology* 80.3, pp. 612–627. DOI: [10.1111/j.1365-2958.2011.07579.x](https://doi.org/10.1111/j.1365-2958.2011.07579.x).
- Taheri-Araghi, Sattar et al. (May 2017). "Cell-Size Control and Homeostasis in Bacteria". en. In: *Current Biology* 27.9, p. 1392. DOI: [10.1016/j.cub.2017.04.028](https://doi.org/10.1016/j.cub.2017.04.028).
- Ursell, Tristan et al. (Dec. 2017). "Rapid, Precise Quantification of Bacterial Cellular Dimensions across a Genomic-Scale Knockout Library". en. In: *BMC Biology* 15.1, p. 17. DOI: [10.1186/s12915-017-0348-8](https://doi.org/10.1186/s12915-017-0348-8).
- Webber, M. A. (Jan. 2003). "The Importance of Efflux Pumps in Bacterial Antibiotic Resistance". In: *Journal of Antimicrobial Chemotherapy* 51.1, pp. 9–11. DOI: [10.1093/jac/dkg050](https://doi.org/10.1093/jac/dkg050).
- Wright, G (July 2005). "Bacterial Resistance to Antibiotics: Enzymatic Degradation and Modification". en. In: *Advanced Drug Delivery Reviews* 57.10, pp. 1451–1470. DOI: [10.1016/j.addr.2005.04.002](https://doi.org/10.1016/j.addr.2005.04.002).